



## Slender-jet equations with surface rheological effects and the Newtonian limit

Hansol Wee, Ajay Harishankar Kumar , Naresh K. Dhanwani, and Osman A. Basaran \*  
*Davidson School of Chemical Engineering, Purdue University, West Lafayette, Indiana 47907, USA*



(Received 31 August 2024; accepted 25 October 2024; published 15 November 2024; corrected 11 December 2024)

Slender-jet equations are a set of nonlinear evolution equations that arise in the analysis of pinch-off singularities and govern the shape of and the axial velocity at leading order within a thinning liquid thread. Moreover, because they are a set of relatively simple transient partial differential equations that depend only on one spatial variable, they are also widely employed in simulating dripping and jetting from nozzles, dynamics of liquid bridges, and contraction of liquid filaments as their use results in drastic reduction in computational effort compared to solving the full set of equations governing such free surface flows. Here, a physically based derivation of the slender-jet equations is presented for situations in which the jet's surface is covered with surfactant and surface rheological (viscous) effects are important and, moreover, both the bulk fluid and the interface can be non-Newtonian. It is worth noting that a derivation of the general slender-jet equations governing the dynamics of jets consisting of arbitrary bulk and surface phases has heretofore been lacking in the literature and this deficiency is hence remedied in this paper. These general equations are then reduced to ones governing the dynamics of what is referred to as a Newtonian jet, i.e., a jet where the bulk liquid is an incompressible Newtonian fluid and its interface is a two-dimensional Newtonian fluid whose rheology is described by the widely used Boussinesq-Scriven constitutive equation. The one-dimensional (1D) slender-jet equations have recently been used to analyze the stability and breakup of primarily Newtonian jets but also of jets of non-Newtonian fluids with a Newtonian surface phase. However, most of the aforementioned studies have been carried out without benchmarking the results obtained from solving the 1D slender-jet equations against full free surface flow simulations or experiments. Therefore, we also present here a comparison of theoretical predictions obtained from slender-jet theory with computational results obtained from the use of a fully three-dimensional, axisymmetric (3DA) algorithm for a breaking surfactant-covered Newtonian jet first when the jet is undergoing Stokes flow and then also when inertia cannot be neglected. For Newtonian jets, analytical results obtained from slender-jet theory are shown to be in excellent accord with predictions obtained from the 3DA simulations.

DOI: [10.1103/PhysRevFluids.9.113602](https://doi.org/10.1103/PhysRevFluids.9.113602)

### I. INTRODUCTION

Breakup of liquid jets, drops, and bridges has been studied continuously for nearly two centuries given the importance of the subject in industrial applications and natural phenomena as diverse as ink jet printing, microarraying, crop spraying, atomization coating, measuring physical properties including surface tension as well as shear and extensional viscosity, and fountains and waterfalls [1–9]. The thinning and breakup of fluid threads undergoing incompressible flow are governed

---

\*Contact author: [obasaran@purdue.edu](mailto:obasaran@purdue.edu)

by the fully three-dimensional (3D) or, for axisymmetric flow, the 3D but axisymmetric (3DA) free boundary problem (or free surface flow) that is comprised of the Cauchy momentum and continuity equations in the bulk and traction and kinematic boundary conditions at the interface [10–13]. In the last three decades, it has been discovered that as the hydrodynamic space-time pinch-off singularity is approached, i.e., in the vicinity of the location where a fluid thread will break, these equations reduce to a set of one-dimensional (1D), lubrication-type equations referred to as the slender-jet equations [14]. Slender-jet equations have been derived and used for both Newtonian and complex fluids for several decades (see below). However, more recently, there has been growing interest in using the slender-jet equations to analyze the dynamics of thread breakup in situations when the interface separating a fluid thread from its surroundings is covered with surfactants and surface rheological or viscous effects are important [15–20]. The goal of this paper is twofold. The first goal is to present a physically based derivation of the slender-jet equations for situations in which the jet’s surface is not only covered with surfactant but surface rheological (viscous) effects are of paramount importance and, moreover, both the bulk fluid and the interface are non-Newtonian. As further discussed below, it is worth noting that a derivation of the general slender-jet equations governing the dynamics of jets consisting of arbitrary bulk and surface phases has heretofore been lacking in the literature and this deficiency is hence remedied in this paper. The second goal is to provide a much needed but also heretofore often lacking direct comparison between predictions obtained from slender-jet theory with computational results obtained from the solution of the full set of equations governing the free surface flow problem of thread pinch-off. Such a comparison is provided here in the most common and hence most often studied situation in which both the bulk and the surface phases are Newtonian.

As numerically solving a set of 1D equations is both less arduous and orders of magnitude faster than solving a set of 3D or 3DA equations, the slender-jet equations have also often been used to simulate the flow in the entire domain and where the slenderness assumption may not hold everywhere. For example, the slender-jet equations have been used to model drop formation by dripping at low flow rates and jetting at higher ones in analyzing the nonlinear dynamics of dripping or leaky faucets [21–27], dynamics of liquid bridges [28–30], and the contraction dynamics of filaments—elongated drops—which are often precursors of undesirable satellite droplets in applications [31–36].

Although lubrication-type equations taking advantage of the slenderness of jets have been around in one form or another for many years [37,38], their use has taken off after the publication of papers by Eggers [14] and Eggers and Dupont [21] on Newtonian pinch-off. Since then, slender-jet equations have been used to analyze the pinch-off of non-Newtonian power-law fluids [30,39–42], viscoelastic fluids [7,43–53], jets subjected to electric fields [54–58], surfactant-covered jets in the absence [59–61] and presence [16,18,19,62] of surface rheological effects, and many other physical problems.

Eggers [14], in his landmark paper on the pinch-off singularity in jet breakup, and Eggers and Dupont [21] (see also [63]) expanded all the dependent variables in a Taylor series in the radial coordinate  $r$  taking advantage of the fact that the extent of the radial coordinate is much smaller than that of the axial coordinate  $z$ . Since then, in addition to expanding the dependent variables in a Taylor series in  $r$  [15,59,64], researchers have derived the slender-jet equations by using Taylor-series expansions in the slenderness ratio [65] and more recently by averaging the governing equations across the cross section of the jet [18,66].

In this paper, we adopt a more physically based approach that uses a momentum balance over a macroscopic control volume to derive the slender-jet equations for surfactant-covered jets when surface rheological effects are important. Moreover, we first derive a set of slender-jet equations without assuming that the bulk fluid and the interface are Newtonian; i.e., we do not assume at the outset that in the bulk fluid, the stress tensor and the rate of strain tensor are related by the Newtonian constitutive equation [13], and that at the interface, the constitutive equation that governs the surface viscous stress tensor is the Boussinesq-Scriven constitutive equation [67,68], as has been the case in all of the publications referred to earlier in the paper. We note that although for many years

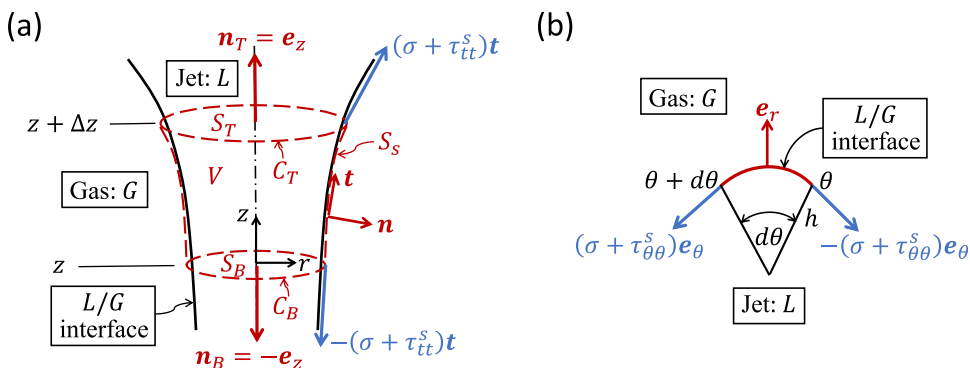


FIG. 1. (a) Control volume (CV) for carrying out a macroscopic force balance on a section of the jet. Here, only surface forces that act on the CV over circular contours of perimeters  $2\pi h$  are shown in the figure. (b) A portion of the interface of differential arclength  $h d\theta$  lying in the  $r\theta$  plane. Once again, only surface forces that act on the two ends of the differential element are shown.

after Sternling and Scriven’s pioneering studies on the effects of surface tension gradients in free surface flows [69–71] and ensuing work by many others on the effects of surface tension gradients in flows involving thin films, liquid drops, and bubbles (see, e.g., [72–75], as examples of recent works on the subject), it is only much more recently that it has become of widespread interest to study the effects of surface rheological or viscous stresses in such free surface flows. Therefore, given this explosion of recent interest [76] and that a derivation of the slender-jet equations for arbitrary bulk and surface phases has heretofore been lacking in the literature, the publication of a paper such as the present one is both desirable and timely. Following the general derivation, we then simplify these equations when the bulk and surface phases are Newtonian. By doing so, we are also able to explain in a simple manner the origin of certain numerical coefficients that appear in these equations. The slender-jet equations have recently been used to analyze the stability and breakup of primarily Newtonian jets [16,18,19,77] but also of jets of non-Newtonian fluids with a Newtonian surface phase [78]. However, most of the aforementioned studies have been carried out without benchmarking the results obtained from solving the 1D slender-jet equations against full free surface flow simulations or experiments. Therefore, we also present here a comparison of theoretical predictions obtained from slender-jet theory with computational results obtained from the use of a fully 3DA algorithm for a breaking surfactant-covered Newtonian jet first when the jet is undergoing Stokes flow and then also when inertia cannot be neglected.

The paper is organized as follows. Section II presents the mathematical statement of the problem. We then derive a general set of equations that take advantage of the slenderness of jets (Sec. III). We next specialize these equations in Sec. IV to Newtonian bulk fluids and where the rheology of the interface is described by the Boussinesq-Scriven model. Section V presents equations of state relating surface tension and surface viscosities to surfactant concentration. In Sec. VI, we provide a brief overview of predictions made with the 1D equations for the pinch-off singularity in the Stokes limit and compare them to ones made with fully 3DA simulations. In the following section (Sec. VII), we allow for the possibility that inertia is important and provide a similar comparison between 1D and fully 3DA predictions. The paper ends in Sec. VIII with some concluding remarks.

## II. MATHEMATICAL FORMULATION

Here, the system is isothermal and consists of a long liquid column (L) (also referred to as a liquid jet or thread) of an incompressible fluid of constant density  $\rho$  that is surrounded by a dynamically passive ambient gas (G) that exerts a constant pressure—which is taken to be the pressure datum—on the column, as shown in Fig. 1(a). The thread’s surface is covered with a monolayer of insoluble

surfactant and the surface tension of the L-G interface is denoted by  $\sigma$ . The dynamics is taken to be axisymmetric about the centerline of the initially cylindrical column of constant radius  $R$ . The jet is vertical and its axis lies parallel to the gravitational acceleration  $\mathbf{g}$ . In what follows, it is convenient to use a cylindrical coordinate system  $(r, \theta, z)$  with its origin located along the centerline of the initially cylindrical column and where  $z$  is the axial coordinate measured along the column's axis in the direction opposite to gravity,  $r$  is the radial coordinate measured from that axis, and  $\theta$  is the usual angle measured around the symmetry axis  $r = 0$ . We also represent the shape of the L-G interface by either using arclength ( $s$ ) parametrization so that  $r = r(s, t)$  and  $z = z(s, t)$  where  $t$  is time or by denoting the interface profile by  $r = h(z, t)$ , where  $h$  is the shape function or the local thread radius. With these two representations, the unit normal and tangent vectors to the jet's surface are given by

$$\mathbf{n} = z_s \mathbf{e}_r - r_s \mathbf{e}_z = \frac{\mathbf{e}_r - h' \mathbf{e}_z}{\sqrt{1 + h'^2}} \quad \text{and} \quad \mathbf{t} = r_s \mathbf{e}_r + z_s \mathbf{e}_z = \frac{h' \mathbf{e}_r + \mathbf{e}_z}{\sqrt{1 + h'^2}}. \quad (1)$$

Here, subscripts  $s$  denote partial differentiation with respect to arclength  $s$ , primes denote partial differentiation with respect to  $z$ , i.e.,  $h' \equiv \partial h / \partial z$ , and  $\mathbf{e}_r$  and  $\mathbf{e}_z$  are the unit vectors in the  $r$  and  $z$  directions. We note that  $r_s^2 + z_s^2 = 1$ ,  $h' = r_s / z_s$ , and  $\sqrt{1 + h'^2} = 1 / z_s$ .

The dynamics of the jet is governed by the continuity and Cauchy momentum equations [11, 79]. The former is given by

$$\nabla \cdot \mathbf{v} = 0, \quad (2)$$

where  $\mathbf{v} = u \mathbf{e}_r + v \mathbf{e}_z$  is the fluid velocity and  $u \equiv \mathbf{v} \cdot \mathbf{e}_r$  and  $v \equiv \mathbf{v} \cdot \mathbf{e}_z$  stand for the radial and axial components of the fluid velocity. Here, we use the integral version of the latter and apply it over the macroscopic control volume  $V$  of height  $\Delta z$  that just cuts the free surface of the jet as shown in Fig. 1(a) and whose lateral or side surface lies in the gas phase just outside the L-G interface:

$$\frac{D}{Dt} \int_V \rho \mathbf{v} dV = \int_S \mathbf{N} \cdot \mathbf{T} dS + \int_V \rho \mathbf{g} dV + \mathbf{F}^s. \quad (3)$$

Here,  $D/Dt$  is the material derivative,  $S$  is the surface that encloses  $V$  with outward pointing unit normal  $\mathbf{N}$ ,  $\mathbf{T}$  is the total bulk stress tensor, and  $\mathbf{F}^s$  are forces due to surface tension and surface rheological (viscous) stresses that act on  $V$  because the control volume cuts the L-G interface (see [11] and below). A slightly different derivation in which the control volume  $V$  does not cut the L-G interface and lies entirely inside the liquid jet is presented in Appendix A.

Equation (3) can be rewritten as

$$\begin{aligned} \int_V \rho \left( \frac{\partial \mathbf{v}}{\partial t} + \mathbf{v} \cdot \nabla \mathbf{v} \right) dV &= \int_{S_s} \mathbf{n} \cdot \mathbf{T}^G dS + \int_{S_T} \mathbf{n}_T \cdot \mathbf{T}^L dS + \int_{S_B} \mathbf{n}_B \cdot \mathbf{T}^L dS \\ &+ \int_V \rho \mathbf{g} dV + \oint_{C_T} \mathbf{t} \cdot \mathbf{T}^s dc + \oint_{C_B} -\mathbf{t} \cdot \mathbf{T}^s dc. \end{aligned} \quad (4)$$

In arriving at Eq. (4), the left-hand side (LHS) of Eq. (3) has been rewritten using a form of the Reynolds transport theorem [13]. The various terms that appear in this equation are discussed in the following few paragraphs.

On the first line of the right-hand side (RHS) of Eq. (4), the surface integral over the surface  $S$  on the RHS of Eq. (3) has been rewritten to explicitly account for the three contributions to it. The first of these is evaluated over area  $S_s$  on the gas side just outside the interface. Here,  $\mathbf{T}^G$  is the bulk stress tensor evaluated on the gas side of the interface and  $\mathbf{n}$  is the unit normal to the L-G interface. We note that  $\mathbf{T}^G = \mathbf{0}$  as the exterior fluid is a passive gas and the pressure in the gas phase  $p^G$  is taken to be the datum level of pressure, i.e.,  $p^G \equiv 0$ . In the second and third of these surface integrals,  $\mathbf{T}^L$  is the total bulk stress tensor in the liquid, and these two integrals are evaluated over the two circular areas  $S_T$ , located at  $z + \Delta z$ , and  $S_B$ , located at  $z$ , with the outward pointing unit normals to each surface being denoted by  $\mathbf{n}_T \equiv \mathbf{e}_z$  and  $\mathbf{n}_B \equiv -\mathbf{e}_z$ . We henceforward drop the superscript ‘‘L’’

and write the total bulk stress in the liquid as  $\mathbf{T} = -p\mathbf{I} + \boldsymbol{\tau}$ , where  $p$  is the pressure,  $\mathbf{I}$  is the identity tensor, and  $\boldsymbol{\tau}$  is the bulk viscous stress tensor.

The integral involving the body force, which accounts for the force due to gravity, has been left unchanged in going from Eq. (3) to Eq. (4).

The force  $\mathbf{F}^s$  in Eq. (3) has been rewritten in Eq. (4) to explicitly show the two contributions to it. In the two line integrals in Eq. (4),  $C_T$  and  $C_B$  are the circular contours bounding  $S_T$  and  $S_B$ ,  $dc$  is the differential arclength along these contours,  $\mathbf{t}$  is the unit tangent to the free surface, and  $\mathbf{T}^s$  is the surface stress tensor given by  $\mathbf{T}^s = \sigma\mathbf{I}^s + \boldsymbol{\tau}^s$ . Here,  $\mathbf{I}^s \equiv \mathbf{I} - \mathbf{n}\mathbf{n}$  is the surface identity tensor and  $\boldsymbol{\tau}^s$  is the surface viscous stress tensor which accounts for surface rheological effects due to surfactants over and beyond their influence on surface tension. For axisymmetric flow,  $\boldsymbol{\tau}^s = \tau_{tt}^s \mathbf{t}\mathbf{t} + \tau_{\theta\theta}^s \mathbf{e}_\theta \mathbf{e}_\theta$ , where  $\mathbf{e}_\theta$  is the unit vector in the  $\theta$  direction. Then,  $\mathbf{t} \cdot \mathbf{T}^s = \sigma\mathbf{t} + \mathbf{t} \cdot \boldsymbol{\tau}^s$  and

$$\begin{aligned} \mathbf{F}^s &= \oint_{C_T} \mathbf{t} \cdot \mathbf{T}^s dc + \oint_{C_B} -\mathbf{t} \cdot \mathbf{T}^s dc = \int_0^{2\pi} (\sigma + \tau_{tt}^s) \mathbf{t} h d\theta \Big|_{z+\Delta z} - \int_0^{2\pi} (\sigma + \tau_{tt}^s) \mathbf{t} h d\theta \Big|_z \\ &= 2\pi h z_s (\sigma + \tau_{tt}^s) \mathbf{e}_z \Big|_{z+\Delta z} - 2\pi h z_s (\sigma + \tau_{tt}^s) \mathbf{e}_z \Big|_z. \end{aligned} \quad (5)$$

Here, in the first line of Eq. (5),  $\pm\sigma\mathbf{t}$  are the usual surface tension forces (per unit length) that act tangential to the interface and perpendicular to the two circular contours each of circumference  $2\pi h$ , and  $\pm\tau_{tt}^s \mathbf{t}$  are the corresponding forces due the surface viscous stresses. In arriving at the second line of Eq. (5), use has been made of the facts that in an axisymmetric flow,  $\sigma$ ,  $\tau_{tt}^s$ ,  $h$ ,  $r_s$ , and  $z_s$  do not vary with  $\theta$  and that  $\partial\mathbf{e}_\theta/\partial\theta = -\mathbf{e}_r$  so that

$$\int_0^{2\pi} \mathbf{t} d\theta = \int_0^{2\pi} (r_s \mathbf{e}_r + z_s \mathbf{e}_z) d\theta = r_s \int_0^{2\pi} -\frac{\partial\mathbf{e}_\theta}{\partial\theta} d\theta + z_s \mathbf{e}_z \int_0^{2\pi} d\theta \equiv \mathbf{0} + 2\pi z_s \mathbf{e}_z,$$

which shows as expected on physical grounds that the component of the surface forces in the radial or horizontal direction drop out of the force balance in Eq. (5) on account of axisymmetry after integration over the angle  $\theta$  or over the two contours  $C_T$  and  $C_B$  [see Fig. 1(a)].

We next take the dot product of the macroscopic momentum balance (4) with  $\mathbf{e}_z$  to obtain the  $z$  component of the momentum equation:

$$\begin{aligned} \int_V \rho \left( \frac{\partial v}{\partial t} + \mathbf{v} \cdot \nabla \mathbf{v} \right) dV &= \int_{S_T} T_{zz} dS \Big|_{z+\Delta z} - \int_{S_B} T_{zz} dS \Big|_z - \int_V \rho g dV \\ &+ \frac{2\pi h}{\sqrt{1+h^2}} (\sigma + \tau_{tt}^s) \Big|_{z+\Delta z} - \frac{2\pi h}{\sqrt{1+h^2}} (\sigma + \tau_{tt}^s) \Big|_z. \end{aligned} \quad (6)$$

Additionally, we impose the traction and kinematic boundary conditions at the L-G interface. The former condition is given by

$$\mathbf{n} \cdot \mathbf{T} = \nabla_s \cdot \mathbf{T}^s = 2H\sigma\mathbf{n} + \nabla_s \sigma + \nabla_s \cdot \boldsymbol{\tau}^s, \quad (7)$$

where  $\nabla_s \equiv \nabla - \mathbf{n}(\mathbf{n} \cdot \nabla)$  is the surface gradient operator, which, when the interface profile is axisymmetric, can be written as  $\nabla_s = \mathbf{t} \partial/\partial s + (\mathbf{e}_\theta/r) \partial/\partial\theta$ . Here, the first of three terms on the RHS of Eq. (7) accounts for the capillary pressure  $-2H\sigma$  where  $2H$  is twice the mean curvature,

$$2H = -\nabla_s \cdot \mathbf{n} = \mathbf{n} \cdot \frac{\partial \mathbf{t}}{\partial s} - \frac{1}{r} \mathbf{n} \cdot \mathbf{e}_r = \frac{h''}{(1+h^2)^{3/2}} - \frac{1}{h(1+h^2)^{1/2}} = \kappa_{\text{in}} + \kappa_{\text{out}}, \quad (8)$$

where  $\kappa_{\text{in}}$  and  $\kappa_{\text{out}}$  stand for the in-plane and the out-of-plane curvatures. In Eq. (7), the second term  $\nabla_s \sigma$  is the surface tension gradient or Marangoni stress, and the last term, which is given by

$$\nabla_s \cdot \boldsymbol{\tau}^s = \left[ \frac{\partial}{\partial s} (\tau_{tt}^s) + \frac{(\tau_{tt}^s - \tau_{\theta\theta}^s)}{r} r_s \right] \mathbf{t} + [\tau_{tt}^s \kappa_{\text{in}} + \tau_{\theta\theta}^s \kappa_{\text{out}}] \mathbf{n}, \quad (9)$$

represents the effect of surface viscous forces at the interface.

The second condition at the interface, viz., the kinematic boundary condition, is given by  $\mathbf{n} \cdot (\mathbf{v} - \mathbf{v}_s) = 0$ , where  $\mathbf{v}_s$  is the velocity of points on the interface, and which can be rewritten as

$$\frac{D}{Dt}[r - h(z, t)] = 0 \quad \Rightarrow \quad -\frac{\partial h}{\partial t} + u - v \frac{\partial h}{\partial z} = 0. \quad (10)$$

We next divide Eq. (6) by  $\Delta z$  and let  $\Delta z \rightarrow 0$  to obtain

$$\int_S \rho \left( \frac{\partial v}{\partial t} + \mathbf{v} \cdot \nabla v \right) dS = \frac{\partial}{\partial z} \int_S T_{zz} dS + \frac{\partial}{\partial z} \left[ \frac{2\pi h}{\sqrt{1+h^2}} (\sigma + \tau_{ii}^s) \right] - \int_S \rho g dS, \quad (11)$$

where  $S$  is the cross-section area of the jet at any axial coordinate  $z$ .

To complete the mathematical formulation of the problem, one also needs constitutive equations for the bulk as well as the surface stress tensors (see below). Surface tension and surface rheological stresses depend on the surfactant concentration  $\Gamma$  at the interface. The latter is governed by a convection-diffusion equation [80]:

$$\frac{\partial \Gamma}{\partial t} + \nabla_s \cdot (\Gamma \mathbf{v}) = D_s \nabla_s^2 \Gamma, \quad (12)$$

where  $D_s$  is the surface diffusivity of surfactant. In addition to surface tension, material properties such as surface viscosities that arise in constitutive equations for surface rheological stresses are functions of surfactant concentration  $\Gamma$ . Therefore, equations of state are needed to relate these physical properties to surfactant concentration to complete the mathematical statement of the problem.

### III. SLENDER-JET ANALYSIS

In what follows, we assume that once the column deforms, the axial length scale  $L$  over which significant changes to the thread shape and the flow field occur is much larger than  $R$  so that the slenderness ratio  $\epsilon \equiv R/L \ll 1$  or that  $\partial h/\partial z = O(\epsilon)$ . We next take it that the axial velocity, the pressure, and the bulk normal stresses to leading order do not vary across the cross section of the jet. First, it follows from the continuity equation that the radial velocity to leading order is given by  $u = -(r/2) \partial v/\partial z$ . Physically speaking, that the axial velocity  $v$  is asymptotically independent of the radial coordinate  $r$ , i.e., to leading order  $v = v(z, t)$ , is only valid when the tangential stress  $T_{rz}$  is a factor of  $\epsilon$  smaller than the normal stress  $T_{zz}$  (and  $T_{rr}$ ). Along the line of axisymmetry, viz.,  $r = 0$ ,  $T_{rz} = 0$ . The necessary condition for  $T_{rz}$  to remain  $O(\epsilon|T_{zz}|)$  throughout the thickness of the liquid thread can be deduced from the tangential component of the traction boundary condition (7) or the tangential stress boundary condition

$$\mathbf{t} \cdot (\mathbf{n} \cdot \mathbf{T}) = \mathbf{t} \cdot (\nabla_s \sigma + \nabla_s \cdot \boldsymbol{\tau}^s), \quad (13)$$

where

$$\mathbf{t} \cdot (\mathbf{n} \cdot \mathbf{T}) = \frac{1}{1+h^2} [h'(T_{zz} - T_{rr}) + (1-h^2)T_{rz}]. \quad (14)$$

Thus, the left-hand side of Eq. (13) is of  $O(|T_{rz}|) = O(\epsilon|T_{zz}|)$  in the slender-jet limit. Therefore, the right-hand side of Eq. (13) or the tangential surface excess stress at the interface  $\mathbf{t} \cdot (\nabla_s \sigma + \nabla_s \cdot \boldsymbol{\tau}^s)$  must be  $O(\epsilon|T_{zz}|)$ . For a more formal discussion, we refer the reader to a number of recent publications [81,82]. Moreover, an *a posteriori* justification of the smallness of the tangential stresses at the interface is also provided below for a Newtonian jet.

The  $z$  component of the momentum balance given in Eq. (11) is next simplified by taking advantage of the slenderness ansatz that has just been introduced:

$$\rho \left( \frac{\partial v}{\partial t} + v \frac{\partial v}{\partial z} \right) \pi h^2 = \frac{\partial}{\partial z} (\pi h^2 T_{zz}) + \frac{\partial}{\partial z} [2\pi h (\sigma + \tau_{zz}^s)] - \pi h^2 \rho g, \quad (15)$$

where use has been made of the fact that  $\tau_{zz}^s \equiv \mathbf{e}_z \cdot \boldsymbol{\tau}^s \cdot \mathbf{e}_z = \tau_{tt}^s + O(\epsilon^2)$ . Here, as in earlier momentum balances which involved  $\tau_{tt}^s$  instead of  $\tau_{zz}^s$  before the slenderness assumption was invoked, it is worth noting the value of the numerical coefficient of 2 multiplying the axial surface stress  $\tau_{zz}^s$ . The factor of 2 arises because this force acts over a circle of circumference  $2\pi h$ .

We next write the axial normal stress  $T_{zz}$  as  $T_{zz} = -p + \tau_{zz}$ . The pressure that appears here can be eliminated by taking the dot product of the traction boundary condition (7) with  $\mathbf{n}$ , i.e., evaluating the normal stress boundary condition, noting that in the slender limit,  $ds \approx dz$ ,  $\mathbf{n} \approx \mathbf{e}_r - h'\mathbf{e}_z$ ,  $\mathbf{e}_r \cdot \nabla_s \approx h' \partial/\partial z$ , and

$$\nabla_s \cdot \boldsymbol{\tau}^s = \left[ \frac{\partial}{\partial z}(\tau_{zz}^s) + \frac{(\tau_{zz}^s - \tau_{\theta\theta}^s)}{h} \frac{\partial h}{\partial z} \right] \mathbf{e}_z - \frac{\tau_{\theta\theta}^s}{h} \mathbf{e}_r. \quad (16)$$

Therefore, since  $\mathbf{n} \cdot (\mathbf{n} \cdot \mathbf{T}) = \mathbf{n} \cdot (2H\sigma \mathbf{n} + \nabla_s \sigma + \nabla_s \cdot \boldsymbol{\tau}^s)$ , in the slender limit

$$-p + \tau_{rr} = -\frac{\sigma + \tau_{\theta\theta}^s}{h}. \quad (17)$$

Equation (17), which, in the slender limit, is a radial force balance, can be readily appreciated and also be derived in an alternate manner that requires no knowledge of differential geometry by performing a simple force balance in the  $r\theta$  plane over a portion of the interface spanning an angle  $d\theta$  or a curve of differential arclength  $hd\theta$  [Fig. 1(b)]. In the slender-jet limit where  $\mathbf{n} \approx \mathbf{e}_r$  to leading order,

$$(-p + \tau_{rr})hd\theta \mathbf{e}_r = (\sigma + \tau_{\theta\theta}^s)\mathbf{e}_\theta \Big|_{\theta+d\theta} - (\sigma + \tau_{\theta\theta}^s)\mathbf{e}_\theta \Big|_{\theta} \equiv -(\sigma + \tau_{\theta\theta}^s)\mathbf{e}_r d\theta,$$

where, in arriving at the final result, use has been made of the facts that in an axisymmetric flow,  $\sigma$  and  $\tau_{\theta\theta}^s$  cannot vary with  $\theta$  and that  $\partial \mathbf{e}_\theta / \partial \theta = -\mathbf{e}_r$ . This balance shows that surface hoop stress  $\tau_{\theta\theta}^s$  gives rise to a resultant in the negative radial direction just like surface tension. We further note that the value of the numerical coefficient that multiplies the surface hoop stress  $\tau_{\theta\theta}^s$  is unity in contrast to the coefficient of 2 that multiplied the surface axial stress  $\tau_{zz}^s$  (see above).

Therefore, after using Eq. (17), the momentum equation can be recast as

$$\rho \left( \frac{\partial v}{\partial t} + v \frac{\partial v}{\partial z} \right) \pi h^2 = \frac{\partial}{\partial z} \left\{ \pi h^2 \left[ (\tau_{zz} - \tau_{rr}) - \frac{\sigma + \tau_{\theta\theta}^s}{h} \right] \right\} + \frac{\partial}{\partial z} [2\pi h (\sigma + \tau_{zz}^s)] - \pi h^2 \rho g. \quad (18)$$

Following division by the cross-section area  $\pi h^2$ , Eq. (18) can be rearranged as

$$\rho \left( \frac{\partial v}{\partial t} + v \frac{\partial v}{\partial z} \right) = \frac{1}{h^2} \left\{ \frac{\partial}{\partial z} [h^2 (\tau_{zz} - \tau_{rr})] + \frac{\partial}{\partial z} (\sigma h) + \frac{\partial}{\partial z} [\mathbf{h}(2\tau_{zz}^s - \tau_{\theta\theta}^s)] \right\} - \rho g. \quad (19)$$

In the final form of the 1D momentum equation, the contributions due to surface viscous effects, i.e., the last of the three terms in curly braces on the RHS of Eq. (19), have been highlighted in bold. It is worth commenting on both the bulk and surface viscous stress terms in this equation before moving forward. Consider a portion of the jet that is nearly cylindrical in shape. Bulk axial extensional stresses  $\tau_{zz}$  stretch the element in the axial direction. However, to conserve mass (volume), the nearly cylindrical element of volume must then be compressed in the radial direction. These observations help rationalize why the bulk viscous stresses enter the momentum balance as the difference between the two primary normal stresses, viz., as the axial bulk viscous stress  $\tau_{zz}$ , which is extensional when  $\partial v / \partial z > 0$ , minus the radial bulk viscous stress,  $\tau_{rr}$ , which in that case is compressional. The term involving the surface viscous stresses can also be rationalized in an analogous manner. First, as with the components of the bulk viscous stress tensor, the two components of the surface stress tensor enter the momentum balance as the difference between the contribution coming from the surface viscous axial stress  $\tau_{zz}^s$  and that due to the surface viscous hoop stress  $\tau_{\theta\theta}^s$ . However, whereas the former is multiplied by 2, the latter is multiplied by 1. The detailed



derivation provided above makes plain why there is a factor of 2 multiplying  $\tau_{zz}^s$ . In the macroscopic force balance,  $\tau_{zz}^s$  enters the balance through a line tension type of contribution where it acts over a circular contour of perimeter  $2\pi h$  whereas  $\tau_{\theta\theta}^s$  enters the balance when the pressure, which acts over the cross section of the jet of area  $\pi h^2$ , is eliminated by replacing it with the sum of contributions due to the surface viscous hoop stress, surface tension, and bulk viscous radial stress after making use of the normal component of the traction boundary condition. However,  $\tau_{\theta\theta}^s$  can be positive or negative even if the flow is extensional as surface area, unlike volume, does not have to remain constant as the jet deforms. Lastly, it is also worth commenting on why the surface tension term has a numerical coefficient of unity associated with it as opposed to the coefficient of 2 that multiplies the surface viscous axial stress. We note that, in going from Eq. (18) to Eq. (19), the factor of 2 that arose in the surface tension term after accounting for the line tension type of contributions along the two contours  $C_T$  and  $C_B$ , a term with the opposite sign but which is multiplied by unity also came into the picture when the pressure in the jet was eliminated in favor of the sum of the surface tension pressure and the surface viscous hoop stress [see the radial force balance (17)]. We also note that the terms involving the contributions from the various surface forces to the 1D momentum balance (19) can be combined and be written as  $\frac{\partial}{\partial z} \{h[\sigma + (2\tau_{zz}^s - \tau_{\theta\theta}^s)]\} = \frac{\partial}{\partial z} \{h^2[\frac{\sigma}{h} + \frac{(2\tau_{zz}^s - \tau_{\theta\theta}^s)}{h}]\}$ , two alternate but equivalent forms that are helpful in enhancing the intuitive understanding of the various forces at play.

To determine the fluid velocity and the interface shape in the slender-jet limit, the 1D momentum equation must be solved along with the 1D mass balance and the convection-diffusion equation for surfactant transport along the interface. The former follows from combining the kinematic boundary condition with the expression for the radial velocity in a slender jet:

$$\frac{\partial h}{\partial t} + v \frac{\partial h}{\partial z} + \frac{h}{2} \frac{\partial v}{\partial z} = 0. \quad (20)$$

The latter for slender flow is given, albeit without any details, in [19]:

$$\frac{\partial \Gamma}{\partial t} + v \frac{\partial \Gamma}{\partial z} + \frac{\Gamma}{2} \frac{\partial v}{\partial z} - \frac{D_s}{h} \frac{\partial}{\partial z} \left( h \frac{\partial \Gamma}{\partial z} \right) = 0. \quad (21)$$

A detailed derivation of Eq. (21) is provided in Appendix B.

#### IV. SLENDER-JET EQUATIONS FOR A NEWTONIAN BULK FLUID AND BOUSSINESQ-SCRIVEN SURFACE FLUID

In this section, the aforementioned equations will be cast into a form when the liquid thread is an incompressible Newtonian fluid so that  $\boldsymbol{\tau} = \mu[\nabla \mathbf{v} + (\nabla \mathbf{v})^T]$ , where  $\mu$  is the bulk viscosity and the surface rheology can be described by the Boussinesq-Scriven constitutive equation [13,67,68]:

$$\boldsymbol{\tau}^s = (\mu_d - \mu_s)(\nabla_s \cdot \mathbf{v})\mathbf{I}_s + \mu_s[\nabla_s \mathbf{v} \cdot \mathbf{I}_s + \mathbf{I}_s \cdot (\nabla_s \mathbf{v})^T], \quad (22)$$

where  $\mu_d$  and  $\mu_s$  are surface dilatational and shear viscosities.

For axisymmetric flow, it is readily shown that the nonzero components of the surface stress tensor are given by

$$\tau_{tt}^s = (\mu_d - \mu_s) \left( \frac{h' \frac{\partial u}{\partial z} + \frac{\partial v}{\partial z}}{1 + h^2} + \frac{u}{h} \right) + 2\mu_s \left( \frac{h' \frac{\partial u}{\partial z} + \frac{\partial v}{\partial z}}{1 + h^2} \right), \quad (23)$$

$$\tau_{\theta\theta}^s = (\mu_d - \mu_s) \left( \frac{h' \frac{\partial u}{\partial z} + \frac{\partial v}{\partial z}}{1 + h^2} + \frac{u}{h} \right) + 2\mu_s \frac{u}{h}. \quad (24)$$

A few additional simplifications result because of the slenderness of the jet. Since for a Newtonian fluid  $\tau_{zz} = 2\mu(\partial v/\partial z)$  and  $\tau_{rr} = 2\mu(\partial u/\partial r)$ , when the jet is slender  $\tau_{rr} = -\mu(\partial v/\partial z)$ . Therefore,  $\tau_{zz} - \tau_{rr} = 3\mu(\partial v/\partial z)$ : the numerical coefficient of 3 is now well known and  $3\mu$  is the celebrated Trouton viscosity [37]. Moreover, for a slender jet of a Newtonian fluid, the surface rheological



stresses take on particularly simple forms given by

$$\tau_{zz}^s = \left( \frac{3\mu_s + \mu_d}{2} \right) \frac{\partial v}{\partial z} \quad \text{and} \quad \tau_{\theta\theta}^s = \left( \frac{\mu_d - 3\mu_s}{2} \right) \frac{\partial v}{\partial z}. \quad (25)$$

With the expressions given in Eqs. (25), the momentum equation in the slender-jet limit also takes on a particularly simple form and is given by

$$\rho \left( \frac{\partial v}{\partial t} + v \frac{\partial v}{\partial z} \right) = \frac{3\mu}{h^2} \frac{\partial}{\partial z} \left( h^2 \frac{\partial v}{\partial z} \right) + \frac{1}{h^2} \left[ \frac{\partial}{\partial z} (\sigma h) + \frac{\partial}{\partial z} \left( h \frac{9\mu_s}{2} \frac{\partial v}{\partial z} \right) + \frac{\partial}{\partial z} \left( h \frac{\mu_d}{2} \frac{\partial v}{\partial z} \right) \right] - \rho g, \quad (26)$$

where the contributions due to the surface viscous stresses, i.e., the last two of the three terms in square brackets on the RHS of Eq. (26), have been highlighted in bold. The numerical coefficients multiplying the two surface viscosities differ and the coefficient in the term involving the shear viscosity is larger than that involving the dilatational viscosity because the surface viscous stresses enter the 1D momentum equation as  $2\tau_{zz}^s - \tau_{\theta\theta}^s$ . Recalling Eq. (13), we note from Eq. (26) that the tangential surface excess stress at the interface due to surface tension gradients or Marangoni stresses  $\mathbf{t} \cdot \nabla_s \sigma$  and surface rheological stresses  $\mathbf{t} \cdot (\nabla_s \cdot \boldsymbol{\tau}^s)$  are of  $O(\partial\sigma/\partial z)$  and  $O(\frac{\partial}{\partial z}(\mu_{s,d} \frac{\partial v}{\partial z}))$  where  $\mu_{s,d}$  stands for the larger of  $\mu_s$  or  $\mu_d$ , respectively, in the limit of small  $\epsilon$ . The bulk viscous stress terms in Eq. (26) are of  $O(\frac{\mu}{h} \frac{\partial h}{\partial z} \frac{\partial v}{\partial z}) = O(\frac{\epsilon}{h} T_{zz})$ . Balancing the bulk viscous stresses and the surface excess stress in Eq. (26), it is evident that the tangential surface excess stresses are indeed of  $O(\epsilon|T_{zz}|)$ , which confirms *a posteriori* the assumption made in Sec. III regarding the smallness of tangential stress throughout the thickness of a liquid thread when the thread is slender.

If the two surface viscosities were equal, Eqs. (25) and (26) take on yet even simpler forms given by

$$\tau_{zz}^s = 2\mu_s \frac{\partial v}{\partial z} \quad \text{and} \quad \tau_{\theta\theta}^s = -\mu_s \frac{\partial v}{\partial z}, \quad (27)$$

$$\rho \left( \frac{\partial v}{\partial t} + v \frac{\partial v}{\partial z} \right) = \frac{3\mu}{h^2} \frac{\partial}{\partial z} \left( h^2 \frac{\partial v}{\partial z} \right) + \frac{1}{h^2} \left[ \frac{\partial}{\partial z} (\sigma h) + \frac{\partial}{\partial z} \left( 5\mu_s h \frac{\partial v}{\partial z} \right) \right] - \rho g, \quad (28)$$

where once again the contributions due to the surface viscous stresses, i.e., the last of the two terms in square brackets on the RHS of Eq. (28), have been highlighted in bold. In this last form, the coefficient of 5 in the term involving surface viscosity (cf. [16,18,19]) arises because the contributions of surface viscous stresses to the momentum balance involve  $2\tau_{zz}^s - \tau_{\theta\theta}^s$  and that  $\tau_{zz}^s = -2\tau_{\theta\theta}^s$ , the latter relation having the same form as  $\tau_{zz} = -2\tau_{rr}$  relating the two bulk viscous stresses.

## V. COMPLETION OF THE PROBLEM STATEMENT

The system of equations governing the dynamics when the jet is slender is given by Eqs. (26), (20), and (21). Completion of the problem statement requires equations of state (EOS) for surface tension and the two surface viscosities.

Surface tension as well as the surface shear and the surface dilatational viscosities are all functions of surfactant concentration  $\Gamma$ , viz.,  $\sigma = \sigma(\Gamma)$ ,  $\mu_s = \mu_s(\Gamma)$ , and  $\mu_d = \mu_d(\Gamma)$ . Here, surface tension  $\sigma$  is related to surfactant concentration  $\Gamma$  via the Szyszkowsky equation of state [59,83,84]:

$$\sigma = \sigma_p + \Gamma_m R_g T \ln \left( 1 - \frac{\Gamma}{\Gamma_m} \right) = \sigma_p \left[ 1 + \beta \ln \left( 1 - \frac{\Gamma}{\Gamma_m} \right) \right], \quad (29)$$

where  $\sigma_p$  is the surface tension of the L-G interface when it is free of surfactant,  $\Gamma_m$  is the maximum packing density of surfactant,  $R_g$  is the gas constant,  $T$  is the absolute temperature, and  $\beta \equiv \Gamma_m R_g T / \sigma_p$  is the surfactant strength parameter. Furthermore, it is common to adopt a model for surface viscosities such that they vanish when  $\Gamma = 0$ . The simplest but physically realistic model

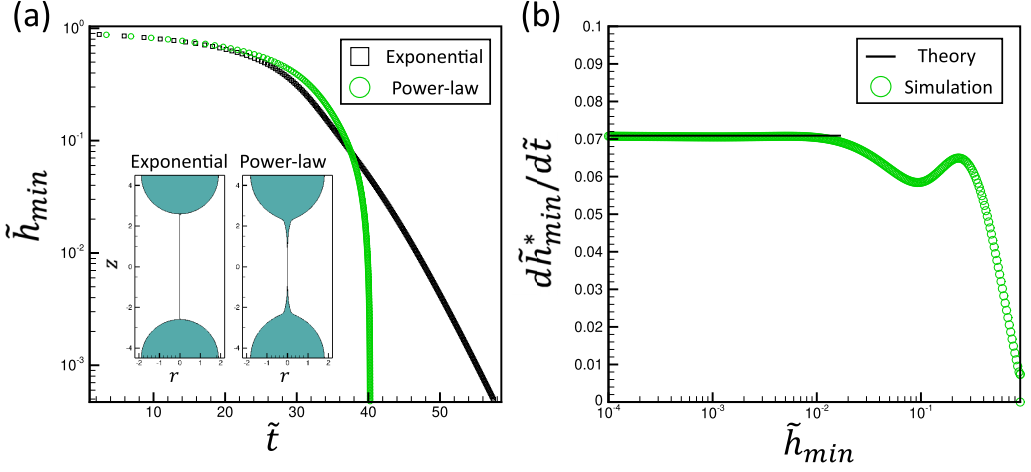


FIG. 2. Computed dynamics of jet thinning obtained from 3DA simulations. (a) Computed variation of dimensionless minimum jet radius  $\tilde{h}_{\min} \equiv h_{\min}/R$  with dimensionless time  $\tilde{t} \equiv t\sigma_p/\mu R$  when  $Pe = 0.9$  (open black squares), which leads to exponential thinning, and  $Pe = 5$  (open green circles), which leads to self-similar dynamics with power-law dependence on time remaining to pinch-off. Shape insets show profiles of jets as  $\tilde{h}_{\min} \rightarrow 0$ . (b) Computed variation of rate of thinning with minimum jet radius when  $Pe = 5$  (open green circles). Here,  $d\tilde{h}_{\min}^*/d\tilde{t} \equiv -\Phi(d\tilde{h}_{\min}/d\tilde{t})$ . The black solid line is the rate of thinning predicted from theory ( $-d\tilde{h}_{\min}^*/d\tilde{t} = 0.0709$ ). Here,  $B_{s0} = 0.1$ ,  $\beta = 0.3$ ,  $\Gamma_0/\Gamma_m = 0.5$ , and  $kR = 0.7$  (dimensionless wavenumber of the initial sinusoidal perturbation imposed on the jet).

for surface viscosity is that it is a linear function of  $\Gamma$ . Therefore, following recent works in the literature [16,18,19,82,85] the surface viscosities are taken to vary linearly with  $\Gamma$  with respect to a reference state as

$$\mu_s = \mu_{s0}\Gamma/\Gamma_0, \quad \mu_d = \mu_{d0}\Gamma/\Gamma_0, \quad (30)$$

where  $\mu_{s0}$  and  $\mu_{d0}$  are the values of the reference surface viscosities at the reference surfactant concentration  $\Gamma_0$ .

## VI. BREAKUP OF STOKES JETS AT LOW AND HIGH PÉCLET NUMBERS

In this section, a short discussion is presented on the breakup of Stokes jets when  $g = 0$  and  $\mu_{d0} \equiv \mu_{s0}$  and a comparison is made between predictions obtained from fully 3DA simulations and slender-jet theory. With Eq. (30), Eq. (28) becomes

$$\frac{\partial}{\partial z} \left[ 3\mu h^2 \frac{\partial v}{\partial z} + \sigma h + 5\mu_{s0} \frac{\Gamma}{\Gamma_0} h \frac{\partial v}{\partial z} \right] = 0. \quad (31)$$

Two limits are of considerable interest: Péclet number  $Pe \equiv R\sigma_p/\mu D_s \rightarrow 0$  ( $Pe$ : relative importance of surfactant convection to diffusion) and  $Pe \rightarrow \infty$ .

When  $Pe \rightarrow 0$ , it has been shown in [16,19] that as the jet thins and  $h \rightarrow 0$ ,  $\Gamma \rightarrow \text{const}$ . Therefore, all variables such as  $\sigma$  and  $\mu_s$  become constants. Since bulk viscous stress varies as  $h^2$  but surface viscous stress varies as  $h$ , the former is asymptotically negligible compared to the latter. Therefore, surface tension and surface viscous forces are in balance as  $h \rightarrow 0$  and it is found that  $\partial v/\partial z \sim \sigma/(5\mu_{s0}\Gamma/\Gamma_0) \equiv \text{const}$ . Substitution of this result into Eq. (20) shows that the minimum radius of the jet,  $h_{\min}$ , tends to zero exponentially in time and the singularity is an infinite-time one [1,9,17,20]. Figure 2(a) shows results from 3DA computations that have been carried out using the

algorithm of [18] that confirm that the thinning is indeed exponential in time as predicted from the theory based on the slender-jet equations [16,19].

When  $Pe \rightarrow \infty$ , it has been shown [16,18,19] that the 1D mass balance and the convection-diffusion equation, Eqs. (20) and (21), become identical in form. Therefore,  $\Gamma \propto h$  or  $\Gamma/\Gamma_m = c_0 h/R$  where  $c_0$  is a constant [18]. Thus, as breakup nears and  $h \rightarrow 0$ ,  $\Gamma \rightarrow 0$  as well. Hence, from a dominant balance argument, the surface tension term in Eq. (31) becomes  $\sigma_p h$  as  $\Gamma \rightarrow 0$  and the 1D momentum equation can be rewritten as

$$\frac{\partial}{\partial z} \left[ 3\mu \frac{\partial v}{\partial z} h^2 \Phi + \sigma_p h \right] = 0, \quad (32)$$

where

$$\Phi = 1 + \frac{5}{3\mu} \mu_{s0} \frac{c_0}{R} \frac{\Gamma_m}{\Gamma_0} = 1 + \frac{5}{3} B_{s0} c_0 \frac{\Gamma_m}{\Gamma_0} \quad (33)$$

and  $B_{s0} \equiv \mu_{s0}/\mu R$  is the Boussinesq-Scriven number. For clean interfaces [65],  $\Phi = 1$ . In this limit, Wee *et al.* [19] have shown that the dynamics in the vicinity of breakup is self-similar and the radial and axial scales,  $h$  and  $z$ , surfactant concentration  $\Gamma$ , and axial velocity  $v$  all have power-law dependencies on time  $\tau \equiv t_b - t$  remaining until pinch-off ( $t_b$ : breakup or pinch-off time). From Eq. (20) or a kinematic balance, it follows that  $v \sim z/\tau$ . From Eq. (31), bulk and surface viscous forces must balance surface tension force,  $h^2 \partial v / \partial z \sim h$ , so that  $h \sim \tau$ . Therefore,  $h \sim \Gamma \sim \tau$ . Furthermore, it follows from Eq. (32) that  $\partial h / \partial \tau \sim \sigma_p / 6\mu \Phi$ . A more exact analysis in [16,19] has shown that

$$h_{\min} = 0.0709(1/\Phi)(\sigma_p/\mu)\tau. \quad (34)$$

Figures 2(a) and 2(b) show results from 3DA computations that have been carried out using the algorithm of [18] that demonstrates that the dynamics indeed exhibits power-law thinning [Fig. 2(a)] and, furthermore, the value of the prefactor obtained from simulations equals 0.0709 in agreement with the theoretical scaling law relating  $h_{\min}$  and  $\tau$  [Fig. 2(b)].

## VII. BREAKUP OF JETS IN THE PRESENCE OF INERTIA AT HIGH PÉCLET NUMBERS

In most situations of interest in practice, typical values of  $Pe$  for jets of aqueous surfactant systems lie in the range  $10^2$ – $10^6$  [83]. Therefore, it is of both practical and fundamental importance to consider jet breakup when inertia cannot be neglected in the limit of large  $Pe$ . In this limit, with Eq. (30), Eq. (28) becomes (cf. Eq. (32) in Stokes flow)

$$\rho \left[ \frac{\partial}{\partial t} (h^2 v) + \frac{\partial}{\partial z} (h^2 v^2) \right] = \frac{\partial}{\partial z} \left[ 3\mu \frac{\partial v}{\partial z} h^2 \Phi + \sigma_p h \right]. \quad (35)$$

Here, the LHS of Eq. (35) is also written in conservation form, similar to its RHS, which can be obtained by multiplying the LHS of Eq. (28) by  $h^2$  and using Eq. (20). The RHS of Eq. (35) remains unchanged from the 1D momentum equation (32) in Stokes flow as the behavior of the local surfactant concentration near breakup is unaltered in the presence of inertia. It has been shown in [18] that the dynamics in the vicinity of breakup in this limit is also self-similar and that  $h \sim \tau$ ,  $\Gamma \sim \tau$ ,  $v \sim \tau^{-1/2}$ , and  $z \sim \tau^{1/2}$ . That  $h \sim \Gamma \sim \tau$  can be easily proved by following the analysis in Sec. VI using the kinematic balance and by balancing the two terms on the RHS of Eq. (35). Balancing inertia with surface tension force, viz.,  $h^2 v^2 \sim h$ , yields  $v \sim \tau^{-1/2}$  and hence  $z \sim \tau^{1/2}$ . Wee *et al.* [18] have also shown that the variation of the minimum jet radius with time remaining to pinch-off in this case is given by

$$h_{\min} = 0.0304(1/\Phi)(\sigma_p/\mu)\tau. \quad (36)$$

Figures 3(a) and 3(b) show results obtained from 3DA computations in the presence of inertia. It is noteworthy that in contrast to the pinch-off of a thread undergoing Stokes flow, breakup when

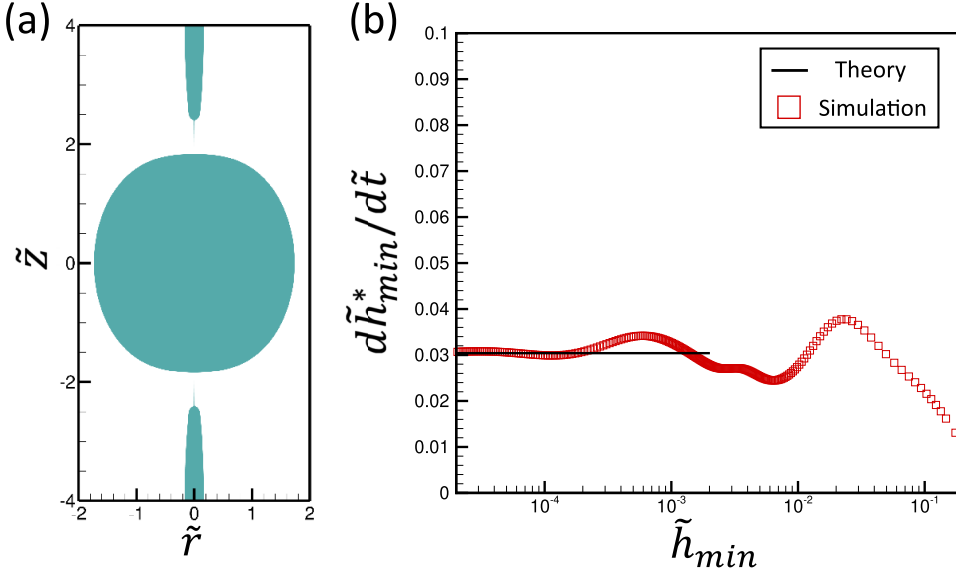


FIG. 3. Computed dynamics of jet thinning obtained from 3DA simulations in the presence of inertia. (a) Computed profile of the jet as  $\tilde{h}_{\min} \rightarrow 0$  provides a stark contrast with jet profiles at the incipience of breakup in Stokes flow. (b) Computed variation of rate of thinning with minimum jet radius (open red squares). Here,  $d\tilde{h}_{\min}^*/d\tilde{t} \equiv -\Phi(d\tilde{h}_{\min}/d\tilde{t})$ . The black solid line is the rate of thinning predicted from theory ( $-d\tilde{h}_{\min}^*/d\tilde{t} = 0.0304$ ). Here,  $Pe = 1000$ ,  $B_{s0} = 0.0143$ ,  $\beta = 0.3$ ,  $\Gamma_0/\Gamma_m = 0.55$ ,  $kR = 0.785$ , and  $Oh = 0.07$ , where  $Oh = \mu/\sqrt{\rho R \sigma_p}$  (note that in Stokes flow,  $1/Oh = 0$ ).

inertia is present occurs asymmetrically [Fig. 3(a)]. Figure 3(b) makes plain that according to the results of the 3DA computations, the dynamics again exhibits power-law behavior in agreement with slender-jet theory. The value of the prefactor obtained from simulations when inertia is present equals 0.0304, which also accords with theory [Fig. 3(b)]. In contrast to pinch-off of a Stokes jet, the approach to the similarity solution in this case exhibits decaying oscillations on account of the dominant complex eigenvalue that dictates the stability of the similarity solution (see the discussion in [86] and [87] for breakup of jets with clean interfaces).

The asymmetric nature of pinch-off when inertia is present as opposed to the symmetric nature of the dynamics in Stokes flow warrants further discussion. That pinch-off occurs asymmetrically in the presence of inertia has now been recognized for more than three decades owing to countless theoretical, computational, and experimental studies [1,4,9,14,18,48,72,83,88–92]. Indeed, the formation of satellite droplets during breakup of liquid columns and filaments but also during dripping and jetting of liquids from nozzles is directly attributable to the asymmetry of pinch-off due to inertia. When inertia is non-negligible, it has been shown in both surfactant-free and surfactant-laden systems that the shape of the interface in the vicinity of the space-time pinch-off singularity is not only self-similar but resembles a thin thread that joins a drop [14,18,72], which is sometimes referred to as the thread-drop solution. It is further known that while the asymmetric similarity solution is valid for a substantial extent of the axial coordinate on the thread side of the axial location where thread radius is minimum, the slope of the interface becomes of order 1 within a much shorter distance on the drop side of the axial location where thread radius is minimum (see, for example, Fig. 5 in [93], Figs. 17 and 18 in [1], and Figs. 1 and 2 in [92], among others). As the slope becomes of order 1 on the drop side, the similarity solution no longer applies, a fact that has already been clearly articulated in the first of Eggers’s seminal review articles on the nonlinear dynamics of free surface flows [1]. However, because asymptotically  $\tilde{h} \sim \tilde{\tau}$ , where  $\tilde{h} \equiv h/R$  and  $\tilde{\tau} \equiv \tau \sigma_p/\mu R$ , and

$\tilde{z} \sim \tilde{\tau}^{1/2}$ , where  $\tilde{z} \equiv z/R$ , in the pinching zone regardless of whether the interface is clean or covered with surfactant, the thread becomes more and more slender as  $\tilde{\tau} \rightarrow 0$  and its aspect ratio grows as  $\tilde{z}/\tilde{h} \sim \tilde{\tau}^{-1/2} \gg 1$  or its slenderness ratio falls as  $\tilde{h}/\tilde{z} \sim \tilde{\tau}^{1/2} \ll 1$ . For example, at  $\tilde{\tau} = 10^{-4}$  dimensionless time units remaining until pinch-off, the dimensionless thread radius would equal to  $10^{-4}$  but the dimensionless axial extent of the pinching zone would equal  $10^{-2}$ . In other words, at that instant, the thread's aspect ratio would equal 100 or its slenderness ratio would equal 0.01. Hence, that the thread remains slender as  $\tilde{\tau} \rightarrow 0$  justifies the use of the slender-jet equations in investigating the dynamics of pinch-off in the presence of inertia shown in Fig. 3.

## VIII. CONCLUSIONS

The physically based derivation of the slender-jet equations governing the dynamics of liquid jets that are covered with surfactant and when surface rheological (viscous) effects are important that is provided in this paper is timely as there is currently an explosive growth of interest in the scientific community in free surface flows in applications ranging from jet breakup to coalescence in which surface rheological effects play an important role [15–19,61,62,82,85,94–97]. While the derivation provided in this paper has been carried out for arbitrary bulk and surface phases, the general equations were subsequently specialized to situations in which the bulk fluid is Newtonian and the rheology of the surface phase is described by the Boussinesq-Scriven constitutive equation [67,68]. The general equations presented in this paper can be readily applied in other situations. For example, Li and Manikantan [77] have used the 1D slender-jet equations to investigate the role of surfactant solubility on the linear stability of Newtonian liquid jets when the effects of surface rheology are modeled by the Boussinesq-Scriven equations (Newtonian interface). In certain applications, the bulk fluid may contain polymer additives so that the jet liquid is a viscoelastic fluid. This situation has recently been considered in a paper by Li and He [78] who used 1D slender-jet equations to primarily study the linearized dynamics of non-Newtonian liquid jets whose bulk rheological responses are governed by either the Oldroyd-B or the FENE-P constitutive models and surface rheological response by the Boussinesq-Scriven model (Newtonian interface). While Li and He [78] and also Li and Manikantan [77] did not do so, their analyses can be further generalized by allowing the interface also to be non-Newtonian. In the Boussinesq-Scriven model considered in Sec. IV, surface viscosities are assumed to be functions solely of surfactant concentration  $\Gamma$ . Such an assumption is applicable when interfaces are covered by relatively simple surfactants or when surfactant concentration is low [76]. However, when the surface is covered by more complex surfactants, e.g., when the interface is comprised of a condensed dipalmitoylphosphatidylcholine (DPPC) monolayer film, surface viscosities can also be functions of strain rate [98]. By allowing surface viscosities to depend on the invariants of the surface stress tensor, the Boussinesq-Scriven model can be generalized to non-Newtonian interfaces, in a manner that is analogous to how the Newtonian fluid model is generalized to power-law or Carreau fluid models that are used to describe bulk rheological responses [99]. However, regardless of the constitutive models chosen to describe the bulk and surface rheological responses, the slender-jet equations would henceforward need not be derived from scratch but instead can be quickly obtained from the general equations provided in Sec. III of this paper.

It should be noted, however, that care must be exercised if the 1D slender-jet equations are used to investigate the linearized and slightly nonlinear dynamics of jets far from breakup. As pointed out by Timmermans and Lister [60], in carrying out a linear stability analysis of a surfactant-covered jet by subjecting an initially perfectly cylindrical column of liquid to small-amplitude disturbances or perturbations, the characteristic equation obtained from the 1D slender-jet equations can fail to capture important changes in the behavior of the growth rate of the perturbations that can occur as the surfactant strength parameter increases. Unless this parameter is small, predictions made with the 1D slender-jet equations can be misleading. In such situations, one must either use a set of 1D slender-jet equations with higher-order corrections, i.e., a theory in which the radial variation of the axial velocity and pressure in the jet are accounted for, or solve the full axisymmetric Navier-Stokes

equations (if the bulk fluid is Newtonian) to investigate the stability of liquid jets. The latter approach has been adopted in this work where the dynamics of jet thinning has been simulated by solving the complete set of 3DA equations from the onset of capillary thinning following the imposition of perturbations until the incipience of pinch-off. The 1D slender-jet equations are only used in this work to provide an analytical description of the dynamics as pinch-off is approached. In summary, the use of 1D slender-jet equations should be avoided when the goal is to analyze the dynamics of capillary thinning and breakup of surfactant-covered liquid threads during the entire duration of the dynamics spanning the period from the onset of thinning until the time when the thread pinches off.

The surface tension of an interface that is covered with surfactant is lower than that compared to the situation when the interface is devoid of surfactant and is reduced by an amount that depends on the local surfactant concentration. There now exist dozens of methods for accurately measuring the surface tension of clean as well as surfactant-covered interfaces (see, e.g., [84,100–103]). When surface rheological effects cannot be neglected, the standard approach, which has also been adopted in the latter part of this paper, has consisted of describing the interface as a compressible two-dimensional Newtonian fluid with surface shear and dilatational viscosities obeying the Boussinesq-Scriven equations [67,68]. However, in contrast to the measurement of surface tension, measurement of material properties of interfaces has proven to be much more challenging [104]. Stevenson [105], for example, has succinctly summarized in a review article that researchers have reported measured values of surface shear viscosity that differ by orders of magnitude. One possible source of difficulty and hence a culprit for the discrepancies in measurements may be that many experimental methods generate a mixed interfacial flow, with both shear and dilatational components, and the surface shear and dilatational viscosities cannot be uniquely determined from measurements of a single mixed-type flow [106]. Another culprit may be that the interfaces in various flows induced in different laboratory experiments are often subjected to gradients in surface tension which then makes it impossible for all practical purposes to separate the contributions of Marangoni stresses from ones due to surface viscosities. As made evident from the 3DA simulation results reported here that Marangoni stresses do indeed become negligible compared to surface viscous stresses as liquid threads approach pinch-off, jet breakup is a convenient experimental platform for inferring surface viscosities by using Eq. (34) or Eq. (36) that have both been obtained from slender-jet theory under the *a priori* assumption that Marangoni stresses are negligible [107].

In a number of equations such as the 1D momentum equation (26), the two surface viscosities appear in combination as  $(9\mu_s + 5\mu_d)/2$ . Therefore, it would be natural to refer to this combination as the effective surface viscosity. However, this combination results solely because of the cylindrical nature of the physical problem at hand. By way of contrast, in sheet rupture [82], the two surface viscosities come into play as the sum of the surface viscosities, viz., as  $\mu_s + \mu_d$ , and it would be natural in that situation to refer to the sum of the two surface viscosities as the effective surface viscosity. Clearly, one can perform experiments involving both jet breakup and sheet rupture to infer the individual values of the two surface viscosities.

## ACKNOWLEDGMENTS

The authors thank the Purdue Process Safety and Assurance Center (P2SAC) and the Purdue Multiphase Flow Center (PMULFLOW), and the Burton and Kathryn Gedge Professorship to OAB for financial support.

## APPENDIX A: DERIVATION OF THE MOMENTUM EQUATION USING A CONTROL VOLUME THAT LIES ENTIRELY WITHIN THE LIQUID JET

Here, we present a derivation of the momentum equation using a macroscopic control volume  $V$  of height  $\Delta z$  that, unlike the control volume of Fig. 1(a), does not cut the free surface of the jet and

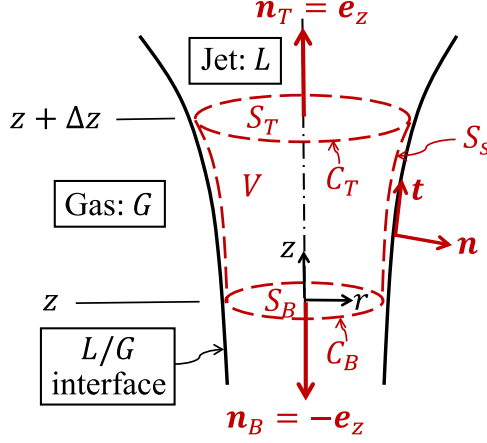


FIG. 4. Control volume (CV) for carrying out a macroscopic force balance on a section of the jet. Unlike the control volume shown in Fig. 1(a), there are no surface forces in this case that act on the CV as it lies entirely within liquid jet.

whose lateral or side surface  $S_s$  lies in the liquid phase just inside the L-G interface (Fig. 4):

$$\frac{D}{Dt} \int_V \rho \mathbf{v} dV = \int_S \mathbf{N} \cdot \mathbf{T} dS + \int_V \rho \mathbf{g} dV. \quad (\text{A1})$$

It should be noted that, unlike Eq. (3), Eq. (A1) does not contain a term  $\mathbf{F}^s$  accounting for line tension type of forces because the control volume lies entirely in the liquid phase and does not intersect the free surface. Following the analysis in Sec. II, the LHS of Eq. (A1) is next simplified using the Reynolds transport theorem, and the surface integral term on the RHS is rewritten to express the different contributions to it:

$$\int_V \rho \left( \frac{\partial \mathbf{v}}{\partial t} + \mathbf{v} \cdot \nabla \mathbf{v} \right) dV = \int_{S_s} \mathbf{n} \cdot \mathbf{T}^L dS + \int_{S_T} \mathbf{n}_T \cdot \mathbf{T}^L dS + \int_{S_B} \mathbf{n}_B \cdot \mathbf{T}^L dS + \int_V \rho \mathbf{g} dV. \quad (\text{A2})$$

We next simplify Eq. (A2) by means of the traction boundary condition

$$\mathbf{n} \cdot \mathbf{T}^L = \mathbf{n} \cdot \mathbf{T}^G + \nabla_s \cdot \mathbf{T}^s \quad (\text{A3})$$

and thereby obtain

$$\begin{aligned} \int_V \rho \left( \frac{\partial \mathbf{v}}{\partial t} + \mathbf{v} \cdot \nabla \mathbf{v} \right) dV &= \int_{S_s} \mathbf{n} \cdot \mathbf{T}^G dS + \int_{S_T} \mathbf{n}_T \cdot \mathbf{T}^L dS + \int_{S_B} \mathbf{n}_B \cdot \mathbf{T}^L dS \\ &\quad + \int_V \rho \mathbf{g} dV + \int_{S_s} \nabla_s \cdot \mathbf{T}^s dS. \end{aligned} \quad (\text{A4})$$

The second surface integral over  $S_s$  can be simplified by means of the surface divergence theorem (SDT) [11] which can be generalized to tensors  $\mathbf{\Omega}$  of any order:

$$\int_{S_s} (\nabla_s \cdot \mathbf{\Omega} + 2H \mathbf{n} \cdot \mathbf{\Omega}) dS = \int_C \mathbf{m} \cdot \mathbf{\Omega} dc, \quad (\text{A5})$$

where  $C$  is (are) the contour(s) bounding the open surface  $S_s$  and  $\mathbf{m}$  is the unit vector that is tangent to  $S_s$  and outwardly normal to  $C$  [11]. When Eq. (A5) is applied to the present problem where  $\mathbf{\Omega} \equiv \mathbf{T}^s$ ,  $C$  consists of  $C_T$  and  $C_B$ ,  $\mathbf{m} = \mathbf{t}$  for  $C_T$  but  $\mathbf{m} = -\mathbf{t}$  for  $C_B$ , and that  $\mathbf{n} \cdot \mathbf{T}^s = \mathbf{0}$ , it is found



that

$$\int_{S_s} \nabla_s \cdot \mathbf{T}^s dS = \oint_{C_T} \mathbf{t} \cdot \mathbf{T}^s dc + \oint_{C_B} -\mathbf{t} \cdot \mathbf{T}^s dc. \quad (\text{A6})$$

When Eq. (A6) is used in Eq. (A4), the resulting equation is identical to Eq. (4).

## APPENDIX B: DERIVATION OF THE SURFACTANT TRANSPORT EQUATION IN THE SLENDER-JET LIMIT

In deriving the slender form of the convection-diffusion equation for surfactant transport, we begin by noting the subtle nuances of the partial time derivative in Eq. (12) and the partial time derivative that appears in the standard definition of the material derivative, viz.,  $D/Dt \equiv \partial/\partial t + \mathbf{v} \cdot \nabla$ . The latter is evaluated while holding fixed the spatial coordinate  $\mathbf{x}$ . The former, however, is evaluated while following the normal motion of the surface [13,108], the meaning of which will be clarified shortly. The motion of an evolving surface in an axisymmetric flow can be formally described by a mapping  $\mathbf{x}_s = \mathbf{x}_s(\eta, t)$ , where  $\mathbf{x}_s$  is the position vector of a point on the surface and  $\eta$  denotes a surface (technically, a curve for axisymmetric flow) coordinate. We immediately see that with the aforementioned mapping, there exists an associated velocity field  $(\partial \mathbf{x}_s / \partial t)_\eta$  which is obtained by taking the partial time derivative of  $\mathbf{x}_s$  while  $\eta$  is held constant. When  $(\partial \mathbf{x}_s / \partial t)_\eta$  only has a normal component, viz.,  $(\partial \mathbf{x}_s / \partial t)_\eta = V_l \mathbf{n}$  where  $V_l$  is the magnitude of  $(\partial \mathbf{x}_s / \partial t)_\eta$  or the normal speed of the surface,  $\eta$  is said to be a “fixed” surface coordinate in the surface [13]. It is this surface coordinate that is held constant in the partial time derivative in Eq. (12).

Since we are concerned with the slender form of Eq. (12), it is convenient to parametrize the surface as  $\mathbf{x}_s = \mathbf{x}_s(z, t) = h(z, t)\mathbf{e}_r + z\mathbf{e}_z$ . The associated velocity field is then readily expressed as  $(\partial \mathbf{x}_s / \partial t)_z = h_t \mathbf{e}_r$ , where  $h_t \equiv (\partial h / \partial t)_z$ . This velocity field makes plain that  $z$  cannot be a fixed surface coordinate  $\eta$  because  $\mathbf{e}_r \neq \mathbf{n}$ . Therefore, one should first consider the transformation  $\frac{\partial}{\partial t}|_\eta \rightarrow \frac{\partial}{\partial t}|_z$  before invoking the slenderness approximation. To this end, we note that  $z = z(\eta, t)$ . This relation has an inverse  $\eta = \eta(z, t)$ , and hence  $\Gamma(\eta, t) = \Gamma(\eta(z, t), t)$ . To make further progress, we use the chain rule of differentiation and obtain

$$\left( \frac{\partial \Gamma}{\partial t} \right)_z = \left( \frac{\partial \Gamma}{\partial \eta} \right)_t \left( \frac{\partial \eta}{\partial t} \right)_z + \left( \frac{\partial \Gamma}{\partial t} \right)_\eta, \quad (\text{B1})$$

$$\left( \frac{\partial \mathbf{x}_s}{\partial t} \right)_z = \left( \frac{\partial \mathbf{x}_s}{\partial \eta} \right)_t \left( \frac{\partial \eta}{\partial t} \right)_z + \left( \frac{\partial \mathbf{x}_s}{\partial t} \right)_\eta. \quad (\text{B2})$$

Since  $\mathbf{t} \equiv \frac{\partial \mathbf{x}_s}{\partial \eta} / S_\eta$  where  $S_\eta \equiv |\frac{\partial \mathbf{x}_s}{\partial \eta}|$ ,  $(\partial \mathbf{x}_s / \partial t)_z = h_t \mathbf{e}_r$ ,  $\frac{\partial}{\partial s} = \frac{\partial}{S_\eta \partial \eta}$ , and  $(\partial \mathbf{x}_s / \partial t)_\eta = V_l \mathbf{n}$ , it can be easily shown that

$$\left( \frac{\partial \Gamma}{\partial t} \right)_\eta = \left( \frac{\partial \Gamma}{\partial t} \right)_z - \frac{\partial \Gamma}{\partial s} \left( \frac{\partial h}{\partial t} \right)_z (\mathbf{e}_r \cdot \mathbf{t}). \quad (\text{B3})$$

We will next substitute Eq. (B3) into Eq. (12) but first rewrite that equation as

$$\left( \frac{\partial \Gamma}{\partial t} \right)_\eta + \mathbf{v} \cdot \nabla_s \Gamma + \Gamma \nabla_s \cdot \mathbf{v} = D_s \nabla_s^2 \Gamma. \quad (\text{B4})$$

In proceeding forward, we replace the first term on the LHS of Eq. (B4) with the relation deduced in Eq. (B3) and combine it with the second term on the LHS of Eq. (B4), i.e.,  $\mathbf{v} \cdot \nabla_s \Gamma$ , to obtain

$$\left( \frac{\partial \Gamma}{\partial t} \right)_\eta + \mathbf{v} \cdot \nabla_s \Gamma = \left( \frac{\partial \Gamma}{\partial t} \right)_z - \frac{\partial \Gamma}{\partial s} \left( \frac{\partial h}{\partial t} \right)_z (\mathbf{e}_r \cdot \mathbf{t}) + \mathbf{v} \cdot \nabla_s \Gamma. \quad (\text{B5})$$

Since  $h_t + vh' = u$ ,  $\mathbf{v} \cdot \nabla_s \Gamma = [u(\mathbf{e}_r \cdot \mathbf{t}) + v(\mathbf{e}_z \cdot \mathbf{t})] \frac{\partial \Gamma}{\partial s}$ , and  $\frac{\partial}{\partial s} = \frac{1}{\sqrt{1+h'^2}} \frac{\partial}{\partial z}$ , one can show that

$$\left( \frac{\partial \Gamma}{\partial t} \right)_\eta + \mathbf{v} \cdot \nabla_s \Gamma = \left( \frac{\partial \Gamma}{\partial t} \right)_z + v \frac{\partial \Gamma}{\partial z}. \quad (\text{B6})$$

Had the partial time derivative in Eq. (12) or Eq. (B4) been misinterpreted as  $\frac{\partial}{\partial t}|_z$ , the convection term  $v \partial \Gamma / \partial z$  in Eq. (B6) would instead have turned out to be  $[(uh' + v)/(1 + h'^2)] \partial \Gamma / \partial z$ , which is incorrect [109].

In completing the derivation of the slender form of the convection-diffusion equation, we next turn our attention to the last term on the LHS of Eq. (B4). Using the definition of the surface gradient operator, we obtain

$$\Gamma \nabla_s \cdot \mathbf{v} = \Gamma \mathbf{t} \cdot \left[ \left( \frac{\partial u}{\partial s} \mathbf{e}_r + \frac{\partial v}{\partial s} \mathbf{e}_z \right) \right] + \frac{\Gamma}{h} \mathbf{e}_\theta \cdot \left\{ \frac{\partial}{\partial \theta} \left[ (u \mathbf{e}_r + v \mathbf{e}_z) \right] \right\}. \quad (\text{B7})$$

Exploiting the axisymmetry in the problem, using Eq. (1) to replace the tangent vector with unit vectors along the  $r$  and  $z$  directions, and taking the dot products indicated in Eq. (B7), we obtain

$$\Gamma \nabla_s \cdot \mathbf{v} = \frac{\Gamma h'}{\sqrt{1+h'^2}} \frac{\partial u}{\partial s} + \frac{\Gamma}{\sqrt{1+h'^2}} \frac{\partial v}{\partial s} + \frac{\Gamma v}{h} \left( \mathbf{e}_\theta \cdot \frac{\partial \mathbf{e}_z}{\partial \theta} \right) + \frac{\Gamma u}{h} \left( \mathbf{e}_\theta \cdot \frac{\partial \mathbf{e}_r}{\partial \theta} \right). \quad (\text{B8})$$

Here, it is important to note that [11]

$$\frac{\partial \mathbf{e}_z}{\partial \theta} = 0, \quad \frac{\partial \mathbf{e}_r}{\partial \theta} = \mathbf{e}_\theta, \quad \text{and} \quad \frac{\partial \mathbf{e}_\theta}{\partial \theta} = -\mathbf{e}_r, \quad (\text{B9})$$

which is essential for correctly simplifying the last two terms on the right-hand side of Eq. (B8). We will now invoke the slenderness approximation as has been done in the main text, i.e.,  $h' = \mathcal{O}(\epsilon)$  and  $ds \approx dz$ , and thereby deduce that in the slender limit, the last term on the LHS of Eq. (B4) reduces to

$$\Gamma \nabla_s \cdot \mathbf{v} \approx \Gamma \frac{\partial v}{\partial z} + \frac{\Gamma u}{h}. \quad (\text{B10})$$

Furthermore, in the slender-jet approximation, the radial velocity  $u = -\frac{h}{2} \frac{\partial v}{\partial z}$  can be used to simplify Eq. (B10) as

$$\Gamma \nabla_s \cdot \mathbf{v} \approx \Gamma \frac{\partial v}{\partial z} - \frac{\Gamma}{2} \frac{\partial v}{\partial z} \equiv \frac{\Gamma}{2} \frac{\partial v}{\partial z}. \quad (\text{B11})$$

Next, we will simplify the diffusion term from Eq. (B4):

$$D_s \nabla_s^2 \Gamma = D_s \nabla_s \cdot (\nabla_s \Gamma) = D_s \nabla_s \cdot \left( \mathbf{t} \frac{\partial \Gamma}{\partial s} + \frac{1}{h} \mathbf{e}_\theta \frac{\partial \Gamma}{\partial \theta} \right). \quad (\text{B12})$$

Due to the axisymmetric nature of the problem, the last term on the RHS of Eq. (B12) is zero. Hence, we obtain

$$D_s \nabla_s^2 \Gamma = D_s \nabla_s \cdot \left( \mathbf{t} \frac{\partial \Gamma}{\partial s} \right) = D_s \left[ \mathbf{t} \cdot \frac{\partial}{\partial s} \left( \mathbf{t} \frac{\partial \Gamma}{\partial s} \right) + \frac{\mathbf{e}_\theta}{h} \cdot \frac{\partial}{\partial \theta} \left( \mathbf{t} \frac{\partial \Gamma}{\partial s} \right) \right]. \quad (\text{B13})$$

The previous equation can be readily simplified by taking advantage of the fact that  $\mathbf{t}$  is a unit tangent vector, i.e.,  $\mathbf{t} \cdot \mathbf{t} = 1$ . Differentiation of the latter relation with respect to arclength allows one to conclude that  $\mathbf{t} \cdot \partial \mathbf{t} / \partial s = 0$ . Combining this result with Eq. (B13), we obtain

$$D_s \nabla_s^2 \Gamma = D_s \left( \frac{\partial^2 \Gamma}{\partial s^2} + \frac{\mathbf{e}_\theta}{h} \frac{\partial \Gamma}{\partial s} \cdot \frac{\partial \mathbf{t}}{\partial \theta} \right). \quad (\text{B14})$$

Following the steps in the analysis carried out previously for the convection terms, we simplify Eq. (B14) using Eqs. (1) and (B9), and thereby obtain

$$D_s \nabla_s^2 \Gamma = D_s \left( \frac{\partial^2 \Gamma}{\partial s^2} + \frac{1}{h} \frac{\partial \Gamma}{\partial s} \frac{h'}{\sqrt{1+h^2}} \right). \quad (\text{B15})$$

Finally, invoking the slenderness approximation, the diffusion term at last simplifies to

$$D_s \nabla_s^2 \Gamma \approx D_s \left( \frac{\partial^2 \Gamma}{\partial z^2} + \frac{\mathbf{h}'}{\mathbf{h}} \frac{\partial \Gamma}{\partial \mathbf{z}} \right) \equiv D_s \frac{1}{h} \frac{\partial}{\partial z} \left( h \frac{\partial \Gamma}{\partial z} \right). \quad (\text{B16})$$

While it may have appeared to the casual reader that the second term that is typeset in bold in the middle formula in Eq. (B16) is negligible in the slender limit, a simple but more careful scaling argument shows that  $\partial^2 \Gamma / \partial z^2$  and  $(h'/h) \partial \Gamma / \partial z$  are in fact of the same order and justifies why both terms have to be retained in the evaluation of the diffusion term:

$$\frac{\partial^2 \Gamma}{\partial z^2} \sim \frac{\Gamma_0}{L^2} \quad \text{and} \quad \frac{h'}{h} \frac{\partial \Gamma}{\partial z} \sim \frac{(R/L) \Gamma_0}{R L} \equiv \frac{\Gamma_0}{L^2}, \quad (\text{B17})$$

where  $\Gamma_0$  is the reference surfactant concentration. Combining all the simplified terms, the surfactant transport equation in the slender limit hence reduces to

$$\frac{\partial \Gamma}{\partial t} + v \frac{\partial \Gamma}{\partial z} + \frac{\Gamma}{2} \frac{\partial v}{\partial z} - \frac{D_s}{h} \frac{\partial}{\partial z} \left( h \frac{\partial \Gamma}{\partial z} \right) = 0. \quad (\text{B18})$$

- 
- [1] J. Eggers, Nonlinear dynamics and breakup of free-surface flows, *Rev. Mod. Phys.* **69**, 865 (1997).
  - [2] O. A. Basaran, Small-scale free surface flows with breakup: Drop formation and emerging applications, *AIChE J.* **48**, 1842 (2002).
  - [3] G. H. McKinley and T. Sridhar, Filament-stretching rheometry of complex fluids, *Annu. Rev. Fluid Mech.* **34**, 375 (2002).
  - [4] J. Eggers and E. Villermaux, Physics of liquid jets, *Rep. Prog. Phys.* **71**, 036601 (2008).
  - [5] O. A. Basaran, H. Gao, and P. P. Bhat, Nonstandard inkjets, *Annu. Rev. Fluid Mech.* **45**, 85 (2013).
  - [6] J. R. Castrejon-Pita, W. R. S. Baxter, J. Morgan, S. Temple, G. D. Martin, and I. M. Hutchings, Future, opportunities and challenges of inkjet technologies, *Atomization Sprays* **23**, 541 (2013).
  - [7] J. Dinic, L. N. Jimenez, and V. Sharma, Pinch-off dynamics and dripping-onto-substrate (DOS) rheometry of complex fluids, *Lab Chip* **17**, 460 (2017).
  - [8] D. Lohse, Fundamental fluid dynamics challenges in inkjet printing, *Annu. Rev. Fluid Mech.* **54**, 349 (2022).
  - [9] C. R. Anthony, H. Wee, V. Garg, S. S. Thete, P. M. Kamat, B. W. Wagoner, E. D. Wilkes, P. K. Notz, A. U. Chen, R. Suryo, K. Sambath, J. C. Panditaratne, Y.-C. Liao, and O. A. Basaran, Sharp interface methods for simulation and analysis of free surface flows with singularities: Breakup and coalescence, *Annu. Rev. Fluid Mech.* **55**, 707 (2023).
  - [10] S. F. Kistler and L. E. Scriven, Coating flows, in *Computational Analysis of Polymer Processing* (Springer, Berlin, 1983), pp. 243–299.
  - [11] W. M. Deen, *Analysis of Transport Phenomena* (Oxford University Press, New York, 1998).
  - [12] L. G. Leal, *Advanced Transport Phenomena: Fluid Mechanics and Convective Transport Processes* (Cambridge University Press, Cambridge, UK, 2007).
  - [13] R. Aris, *Vectors, Tensors and the Basic Equations of Fluid Mechanics* (Dover, New York, 2012).
  - [14] J. Eggers, Universal pinching of 3D axisymmetric free-surface flow, *Phys. Rev. Lett.* **71**, 3458 (1993).
  - [15] A. Martínez-Calvo and A. Sevilla, Temporal stability of free liquid threads with surface viscoelasticity, *J. Fluid Mech.* **846**, 877 (2018).

- [16] H. Wee, B. W. Wagoner, P. M. Kamat, and O. A. Basaran, Effects of surface viscosity on breakup of viscous threads, *Phys. Rev. Lett.* **124**, 204501 (2020).
- [17] A. Martínez-Calvo and A. Sevilla, Universal thinning of liquid filaments under dominant surface forces, *Phys. Rev. Lett.* **125**, 114502 (2020).
- [18] H. Wee, B. W. Wagoner, V. Garg, P. M. Kamat, and O. A. Basaran, Pinch-off of a surfactant-covered jet, *J. Fluid Mech.* **908**, A38 (2021).
- [19] H. Wee, B. W. Wagoner, and O. A. Basaran, Absence of scaling transitions in breakup of liquid jets caused by surface viscosity, *Phys. Rev. Fluids* **7**, 074001 (2022).
- [20] P. Bazazi, H. A. Stone, and S. H. Hejazi, Dynamics of droplet pinch-off at emulsified oil-water interfaces: Interplay between interfacial viscoelasticity and capillary forces, *Phys. Rev. Lett.* **130**, 034001 (2023).
- [21] J. Eggers and T. F. Dupont, Drop formation in a one-dimensional approximation of the Navier–Stokes equation, *J. Fluid Mech.* **262**, 205 (1994).
- [22] X. D. Shi, M. P. Brenner, and S. R. Nagel, A cascade of structure in a drop falling from a faucet, *Science* **265**, 219 (1994).
- [23] B. Ambravaneswaran, S. D. Phillips, and O. A. Basaran, Theoretical analysis of a dripping faucet, *Phys. Rev. Lett.* **85**, 5332 (2000).
- [24] B. Ambravaneswaran, E. D. Wilkes, and O. A. Basaran, Drop formation from a capillary tube: Comparison of one-dimensional and two-dimensional analyses and occurrence of satellite drops, *Phys. Fluids* **14**, 2606 (2002).
- [25] B. Ambravaneswaran, H. J. Subramani, S. D. Phillips, and O. A. Basaran, Dripping-jetting transitions in a dripping faucet, *Phys. Rev. Lett.* **93**, 034501 (2004).
- [26] O. E. Yildirim, Q. Xu, and O. A. Basaran, Analysis of the drop weight method, *Phys. Fluids* **17**, 062107 (2005).
- [27] H. J. Subramani, H. K. Yeoh, R. Suryo, Q. Xu, B. Ambravaneswaran, and O. A. Basaran, Simplicity and complexity in a dripping faucet, *Phys. Fluids* **18**, 032106 (2006).
- [28] R. M. S. M. Schulkes, Dynamics of liquid jets revisited, *J. Fluid Mech.* **250**, 635 (1993).
- [29] X. Zhang, R. S. Padgett, and O. A. Basaran, Nonlinear deformation and breakup of stretching liquid bridges, *J. Fluid Mech.* **329**, 207 (1996).
- [30] O. E. Yildirim and O. A. Basaran, Deformation and breakup of stretching bridges of Newtonian and shear-thinning liquids: Comparison of one-and two-dimensional models, *Chem. Eng. Sci.* **56**, 211 (2001).
- [31] P. K. Notz and O. A. Basaran, Dynamics and breakup of a contracting liquid filament, *J. Fluid Mech.* **512**, 223 (2004).
- [32] T. Driessen, R. Jeurissen, H. Wijshoff, F. Toschi, and D. Lohse, Stability of viscous long liquid filaments, *Phys. Fluids* **25**, 062109 (2013).
- [33] J.-L. Pierson, J. Magnaudet, E. J. Soares, and S. Popinet, Revisiting the Taylor–Culick approximation: Retraction of an axisymmetric filament, *Phys. Rev. Fluids* **5**, 073602 (2020).
- [34] U. Sen, C. Datt, T. Segers, H. Wijshoff, J. H. Snoeijer, M. Versluis, and D. Lohse, The retraction of jetted slender viscoelastic liquid filaments, *J. Fluid Mech.* **929**, A25 (2021).
- [35] X. Liu, B. W. Wagoner, H. Wee, and O. A. Basaran, Effect of initial conditions on promotion and inhibition of breakup during filament contraction, *AIChE J.* **68**, e17491 (2022).
- [36] X. Liu, B. W. Wagoner, and O. A. Basaran, Contraction velocity of viscoelastic filaments, *Phys. Rev. Fluids* **7**, L121601 (2022).
- [37] R. B. Bird, R. C. Armstrong, and O. Hassager, *Dynamics of Polymeric Liquids, Volume 1: Fluid Mechanics*, 2nd ed. (Wiley, New York, 1987).
- [38] A. L. Yarin, *Free Liquid Jets and Films: Hydrodynamics and Rheology* (Longman, Wiley & Sons, Harlow/New York, 1993).
- [39] M. Renardy, Similarity solutions for jet breakup for various models of viscoelastic fluids, *J. Non-Newtonian Fluid Mech.* **104**, 65 (2002).
- [40] P. Doshi, R. Suryo, O. E. Yildirim, G. H. McKinley, and O. A. Basaran, Scaling in pinch-off of generalized Newtonian fluids, *J. Non-Newtonian Fluid Mech.* **113**, 1 (2003).
- [41] P. Doshi and O. A. Basaran, Self-similar pinch-off of power law fluids, *Phys. Fluids* **16**, 585 (2004).

- [42] R. Suryo and O. A. Basaran, Local dynamics during pinch-off of liquid threads of power law fluids: Scaling analysis and self-similarity, *J. Non-Newtonian Fluid Mech.* **138**, 134 (2006).
- [43] D. Bousfield, R. Keunings, G. Marrucci, and M. Denn, Nonlinear analysis of the surface tension driven breakup of viscoelastic filaments, *Chem. Eng. Sci.* **21**, 79 (1986).
- [44] G. H. McKinley and A. Tripathi, How to extract the Newtonian viscosity from capillary breakup measurements in a filament rheometer, *J. Rheol.* **44**, 653 (2000).
- [45] S. L. Anna and G. H. McKinley, Elasto-capillary thinning and breakup of model elastic liquids, *J. Rheol.* **45**, 115 (2001).
- [46] C. Clasen, J. Eggers, M. A. Fontelos, J. Li, and G. H. McKinley, The beads-on-string structure of viscoelastic threads, *J. Fluid Mech.* **556**, 283 (2006).
- [47] P. P. Bhat, O. A. Basaran, and M. Pasquali, Dynamics of viscoelastic liquid filaments: Low capillary number flows, *J. Non-Newtonian Fluid Mech.* **150**, 211 (2008).
- [48] P. P. Bhat, S. Appathurai, M. T. Harris, M. Pasquali, G. H. McKinley, and O. A. Basaran, Formation of beads-on-a-string structures during break-up of viscoelastic filaments, *Nat. Phys.* **6**, 625 (2010).
- [49] A. M. Ardekani, V. Sharma, and G. H. McKinley, Dynamics of bead formation, filament thinning and breakup in weakly viscoelastic jets, *J. Fluid Mech.* **665**, 46 (2010).
- [50] P. P. Bhat, S. Appathurai, M. T. Harris, and O. A. Basaran, On self-similarity in the drop-filament corner region formed during pinch-off of viscoelastic fluid threads, *Phys. Fluids* **24**, 083101 (2012).
- [51] L. N. Jimenez, J. Dinic, N. Parsi, and V. Sharma, Extensional relaxation time, pinch-off dynamics, and printability of semidilute polyelectrolyte solutions, *Macromolecules* **51**, 5191 (2018).
- [52] J. Eggers, M. A. Herrada, and J. H. Snoeijer, Self-similar breakup of polymeric threads as described by the Oldroyd-B model, *J. Fluid Mech.* **887**, A19 (2020).
- [53] C. D. V. Martı́nez N., J. Dinic, X. Lu, C. Wang, R. Rock, H. Sun, and V. Sharma, Rheology and pinching dynamics of associative polysaccharide solutions, *Macromolecules* **54**, 6372 (2021).
- [54] F. J. Garcia, A. Castellanos, and H. Gonzalez, Dynamics of slender viscous dielectric liquid bridges subjected to axial AC fields, *J. Electrostat.* **42**, 259 (1997).
- [55] M. M. Hohman, M. Shin, G. Rutledge, and M. P. Brenner, Electrospinning and electrically forced jets. I. Stability theory, *Phys. Fluids* **13**, 2201 (2001).
- [56] J. J. Feng, The stretching of an electrified non-Newtonian jet: A model for electrospinning, *Phys. Fluids* **14**, 3912 (2002).
- [57] R. T. Collins, M. T. Harris, and O. A. Basaran, Breakup of electrified jets, *J. Fluid Mech.* **588**, 75 (2007).
- [58] S. N. Reznik and E. Zussman, Capillary-dominated electrified jets of a viscous leaky dielectric liquid, *Phys. Rev. E* **81**, 026313 (2010).
- [59] B. Ambravaneswaran and O. A. Basaran, Effects of insoluble surfactants on the nonlinear deformation and breakup of stretching liquid bridges, *Phys. Fluids* **11**, 997 (1999).
- [60] M.-L. E. Timmermans and J. R. Lister, The effect of surfactant on the stability of a liquid thread, *J. Fluid Mech.* **459**, 289 (2002).
- [61] A. Martı́nez-Calvo, J. Rivero-Rodrı́guez, B. Scheid, and A. Sevilla, Natural break-up and satellite formation regimes of surfactant-laden liquid threads, *J. Fluid Mech.* **883**, A35 (2020).
- [62] A. Ponce-Torres, M. A. Herrada, J. M. Montanero, and J. M. Vega, Linear and nonlinear dynamics of an insoluble surfactant-laden liquid bridge, *Phys. Fluids* **28**, 112103 (2016).
- [63] F. J. Garcı́a and A. Castellanos, One-dimensional models for slender axisymmetric viscous liquid jets, *Phys. Fluids* **6**, 2676 (1994).
- [64] Y. E. Kamis, H. B. Eral, and W.-P. Breugem, Active control of jet breakup and droplet formation using temperature modulation, *Phys. Rev. Fluids* **6**, 103903 (2021).
- [65] D. T. Papageorgiou, On the breakup of viscous liquid threads, *Phys. Fluids* **7**, 1529 (1995).
- [66] F. Yang and H. A. Stone, Formation, rupture, and healing of an annular viscous film, *Phys. Rev. Lett.* **124**, 224501 (2020).
- [67] J. Boussinesq, Sur l'existence d'une viscosité superficielle dans la mince couche de transition séparant un liquide d'un autre fluide contigu, *Ann. Chim. Phys.* **29**, 349 (1913).

- [68] L. E. Scriven, Dynamics of a fluid interface equation of motion for Newtonian surface fluids, [Chem. Eng. Sci.](#) **12**, 98 (1960).
- [69] C. V. Sternling and L. E. Scriven, Interfacial turbulence: Hydrodynamic instability and the Marangoni effect, [AIChE J.](#) **5**, 514 (1959).
- [70] L. E. Scriven and C. V. Sternling, The Marangoni effects, [Nature \(London\)](#) **187**, 186 (1960).
- [71] L. E. Scriven and C. V. Sternling, On cellular convection driven by surface-tension gradients: Effects of mean surface tension and surface viscosity, [J. Fluid Mech.](#) **19**, 321 (1964).
- [72] P. M. Kamat, B. W. Wagoner, S. S. Thete, and O. A. Basaran, Role of Marangoni stress during breakup of surfactant-covered liquid threads: Reduced rates of thinning and microthread cascades, [Phys. Rev. Fluids](#) **3**, 043602 (2018).
- [73] P. M. Kamat, B. W. Wagoner, A. A. Castrejón-Pita, J. R. Castrejón-Pita, C. R. Anthony, and O. A. Basaran, Surfactant-driven escape from endpinching during contraction of nearly inviscid filaments, [J. Fluid Mech.](#) **899**, A28 (2020).
- [74] A. Marin, S. Karpitschka, D. Noguera-Marín, M. A. Cabrerizo-Vílchez, M. Rossi, C. J. Kähler, and M. A. R. Valverde, Solutal Marangoni flow as the cause of ring stains from drying salty colloidal drops, [Phys. Rev. Fluids](#) **4**, 041601 (2019).
- [75] D. Lohse and X. Zhang, Physicochemical hydrodynamics of droplets out of equilibrium, [Nat. Rev. Phys.](#) **2**, 426 (2020).
- [76] H. Manikantan and T. M. Squires, Surfactant dynamics: Hidden variables controlling fluid flows, [J. Fluid Mech.](#) **892**, P1 (2020).
- [77] J. Li and H. Manikantan, Stability and thinning of liquid jets in the presence of soluble surfactants, [J. Chem. Phys.](#) **160**, 024902 (2024).
- [78] F. Li and D. He, Dynamics of a surfactant-laden viscoelastic thread in the presence of surface viscosity, [J. Fluid Mech.](#) **966**, A35 (2023).
- [79] S. Whitaker, *Introduction to Fluid Mechanics* (Prentice-Hall, Englewood Cliffs, NJ, 1968).
- [80] H. A. Stone, A simple derivation of the time-dependent convective-diffusion equation for surfactant transport along a deforming interface, [Phys. Fluids](#) **2**, 111 (1990).
- [81] M. Bowen and B. S. Tilley, Thermally induced van der Waals rupture of thin viscous fluid sheets, [Phys. Fluids](#) **24**, 032106 (2012).
- [82] H. Wee, B. W. Wagoner, and O. A. Basaran, Spontaneous rupture of surfactant-covered thin liquid sheets, [Phys. Rev. Fluids](#) **7**, 094005 (2022).
- [83] Y. C. Liao, E. I. Franses, and O. A. Basaran, Deformation and breakup of a stretching liquid bridge covered with an insoluble surfactant monolayer, [Phys. Fluids](#) **18**, 022101 (2006).
- [84] J. C. Berg, *An introduction to Interfaces & Colloids: The Bridge to Nanoscience* (World Scientific, Singapore, 2010).
- [85] A. Ponce-Torres, J. M. Montanero, M. A. Herrada, E. J. Vega, and J. M. Vega, Influence of the surface viscosity on the breakup of a surfactant-laden drop, [Phys. Rev. Lett.](#) **118**, 024501 (2017).
- [86] Y. Li and J. E. Sprittles, Capillary breakup of a liquid bridge: Identifying regimes and transitions, [J. Fluid Mech.](#) **797**, 29 (2016).
- [87] M. C. Dallaston, C. Zhao, J. E. Sprittles, and J. Eggers, Stability of similarity solutions of viscous thread pinch-off, [Phys. Rev. Fluids](#) **6**, 104004 (2021).
- [88] D. H. Peregrine, G. Shoker, and A. Symon, The bifurcation of liquid bridges, [J. Fluid Mech.](#) **212**, 25 (1990).
- [89] Y. J. Chen and P. H. Steen, Dynamics of inviscid capillary breakup: Collapse and pinchoff of a film bridge, [J. Fluid Mech.](#) **341**, 245 (1997).
- [90] R. F. Day, E. J. Hinch, and J. R. Lister, Self-similar capillary pinchoff of an inviscid fluid, [Phys. Rev. Lett.](#) **80**, 704 (1998).
- [91] E. D. Wilkes, S. D. Phillips, and O. A. Basaran, Computational and experimental analysis of dynamics of drop formation, [Phys. Fluids](#) **11**, 3577 (1999).
- [92] A. U. Chen, P. K. Notz, and O. A. Basaran, Computational and experimental analysis of pinch-off and scaling, [Phys. Rev. Lett.](#) **88**, 174501 (2002).
- [93] J. Eggers, Drop formation—an overview, [Z. Angew. Math. Mech.](#) **85**, 400 (2005).

- [94] J. T. Schwalbe, F. R. Phelan, Jr., P. M. Vlahovska, and S. D. Hudson, Interfacial effects on droplet dynamics in Poiseuille flow, [Soft Matter](#) **7**, 7797 (2011).
- [95] A. Ponce-Torres, M. Rubio, M. A. Herrada, J. Eggers, and J. M. Montanero, Influence of the surface viscous stress on the pinch-off of free surfaces loaded with nearly-inviscid surfactants, [Sci. Rep.](#) **10**, 16065 (2020).
- [96] N. Singh and V. Narsimhan, Numerical investigation of the effect of surface viscosity on droplet breakup and relaxation under axisymmetric extensional flow, [J. Fluid Mech.](#) **946**, A24 (2022).
- [97] A. Ponce-Torres, M. Rubio, M. A. Herrada, J. Eggers, and J. M. Montanero, Author correction: Influence of the surface viscous stress on the pinch-of of free surfaces loaded with nearly-inviscid surfactants, [Sci. Rep.](#) **12**, 5744 (2022).
- [98] A. Raghunandan, A. H. Hirs, P. T. Underhill, and J. M. Lopez, Predicting steady shear rheology of condensed-phase monomolecular films at the air-water interface, [Phys. Rev. Lett.](#) **121**, 164502 (2018).
- [99] N. O. Jaensson, P. D. Anderson, and J. Vermant, Computational interfacial rheology, [J. Non-Newtonian Fluid Mech.](#) **290**, 104507 (2021).
- [100] X. Zhang, M. T. Harris, and O. A. Basaran, Measurement of dynamic surface tension by a growing drop technique, [J. Colloid Interface Sci.](#) **168**, 47 (1994).
- [101] E. I. Franses, O. A. Basaran, and C. H. Chang, Techniques to measure dynamic surface tension, [Curr. Opin. Colloid Interface Sci.](#) **1**, 296 (1996).
- [102] Y. M. Tricot, Surfactants: Static and dynamic surface tension, in *Liquid Film Coating: Scientific Principles and their Technological Implications*, edited by S. F. Kistler and P. M. Schweizer (Springer, Dordrecht, Netherlands, 1997), pp. 99–136.
- [103] M. Hoorfar and A. W. Neumann, Recent progress in axisymmetric drop shape analysis (ADSA), [Adv. Colloid Interface Sci.](#) **121**, 25 (2006).
- [104] J. M. Lopez and A. Hirs, Direct determination of the dependence of the surface shear and dilatational viscosities on the thermodynamic state of the interface: Theoretical foundations, [J. Colloid Interface Sci.](#) **206**, 231 (1998).
- [105] P. Stevenson, Remarks on the shear viscosity of surfaces stabilised with soluble surfactants, [J. Colloid Interface Sci.](#) **290**, 603 (2005).
- [106] G. J. Elfring, L. G. Leal, and T. M. Squires, Surface viscosity and Marangoni stresses at surfactant laden interfaces, [J. Fluid Mech.](#) **792**, 712 (2016).
- [107] H. Wee, B. W. Wagoner, P. M. Kamat, V. Garg, and O. A. Basaran, Instrument and method for accurate measurement of surface viscosity of viscous liquid (2024), US Patent No. 12,061,141 (13 August 2024).
- [108] P. Cermelli, E. Fried, and M. E. Gurtin, Transport relations for surface integrals arising in the formulation of balance laws for evolving fluid interfaces, [J. Fluid Mech.](#) **544**, 339 (2005).
- [109] A. Pereira and S. Kalliadasis, On the transport equation for an interfacial quantity, [Eur. Phys. J. Appl. Phys.](#) **44**, 211 (2008).

*Correction:* During the production of proofs, terms in Eqs. (19), (26), (28), and (B16) were set without the intended highlighting. Those terms have now been set in bold and the text following those equations has been adjusted to reflect the change.